Thesis for Ph. D. Degree

Study on Topographic Changes in Tidal Flats of the West Coast of South Korea between 1980s and 2010s Using Remote Sensing Data

원격탐사 자료를 이용한 한국 서해안 조간대의

지형 변화 연구 **(1980s - 2010s)**

Zhen Xu

August 2016

School of Earth and Environmental Sciences

Graduate School

Seoul National University

Study on Topographic Changes in Tidal Flats of the West Coast of South Korea between 1980s and 2010s Using Remote Sensing Data

원격탐사 자료를 이용한 한국 서해안 조간대의 지형 변화 연구 (1980s - 2010s)

지도 교수 김 덕 진

이 논문을 이학박사 학위논문으로 제출함

2016 년 8 월

서울대학교 대학원

지구환경과학부

XU ZHEN

XU ZHEN의 이학박사 학위논문을 인준함

2016 년 8 월

위 원 장 조 양 기 (인)

부위원장 김 덕 진 (인)

위 원 이 효 성 (인)

위 원 박 상 은 (인)

위 원 남 성 현 (인)

Abstract

Morphologic and topologic changes of tidal flats areas have attracted world-wide interest due to their function and importance. In recent times, diverse researches were performed to detect and estimate the temporal topographic changes of tidal flat using various remote sensing data. This study aims to estimate and evaluate topographic changes in Gomso and Hampyeong Bay of South Korea using waterline method and SAR data.

First of all, the seasonal topographic variation in the tidal flat were estimated using the waterline method. A total of 18 scenes of Landsat 7 data acquired during the period from 2003 and 2004 provided individual waterlines for various tidal heights and their corresponding tide gauge observation data defines the reference height. Results showed that summer deposition is a main dominant effect in tidal flats in Gomso Bay with an average overall seasonal topographic change of 12.8 cm. In contrast, summer erosion is dominant with -5.0 cm topographic variation in Hampyeong Bay. Although both Gomso and Hampyeong Bay are classified as semi-enclosed coast tidal flat, the sedimentary facies caused by formation geometry and sediment type led to different topographic changes.

Secondly, topographic changes were estimated from DEMs generated for the years 1980s and 2010s using the waterline method, Seasonal topographic changes was taken into consideration to estimate the minimum topographic changes of each bay in the study area. As a result, during1980s and 2010s Gomso Bay showed the

predominant deposition regardless of the season. In the winter, the amount of deposition was about 12.4 cm; in the summer, the deposition was about 31.9 cm. For Hampyeong Bay, erosion was dominant in overall with the amount of 29.6 cm and 41.2 cm in the summer and winter, respectively, in the past 30 years.

The waterline method is unique way of extract the topographic information in the past few decades. Furthermore, the temporal topographic changes during 1980s to 2010s have been analyzed. A total of 82 scenes of Landsat 2, 3, 4, 5, 7 and 8 images were used to extract the waterline and generate the DEM with winter and summer during the past 30 years (1980-2010) in the Gomso and Hampyeong Bay. From the results, the temporal topographic changes have shown clear seasonal characteristics in the winter and summer during the past 30 years, in the Gomso and Hapyeong Bay. As the 2000s the topographic was not regularly deposed and eroded, in the Gomso and Hampyeong Bay. It might be also effect on constructed big Saemangum sea dyke.

Finally, the feasibility of SAR interferometry technique for monitoring topographic variation in tidal flats has been evaluated. The topography of tidal flats in Gomso Bay derived from TanDEM-X bi-static interferometry and SRTM mission data are compared with those from the waterline method. Although the temporal difference between the datasets prevented from direct topographic comparison, the spatial trends of deposition and erosion were similar to those from the waterline method. It is highly expected that monitoring topographic variation of tidal flats using SAR interferometry will become practically possible if more single-pass interferometry SAR data are collected in time series.

This research is the first approach of detecting seasonal topographic variations by the waterline method. Consideration of the seasonal topographic changes is essentially important in detecting more accurate long term topographic changes in the tidal flat. By using the waterline method, it is more easy to restore the past DEM. From the effective analysis and understanding of the long term topographic changes, we can able to respond more rapidly to current and future coastal environmental changes.

Keywords: Waterline method, Tidal flats, Seasonal variations, Topography changes, Remote sensing.

Student Number: 2011-31269

List of Contents

List of Figures

List of Tables

Chapter 1. Introduction

1. Background

Tidal flats are integrated systems that inundated during high tide and exposed during low tide (Figure 1-1). They are similar to the intertidal zone. However, their motion is closely related to the mass exchanges with the supratidal and subtidal zone. All tidal flat systems, except those in areas dominated by wind tide, are composed of three basic environments: supratidal, intertidal and subtidal. (Chen, 2000; Li et al., 2005; Reineck et al., 1980; Shinn 1983).

The three zones in a tidal flat are defined as: 1) the supratidal zone, located above high tide mark; 2) the intertidal zone, located between high and low tide marks; and 3) the subtidal zone which occurs below low tide mark and is rarely exposed.

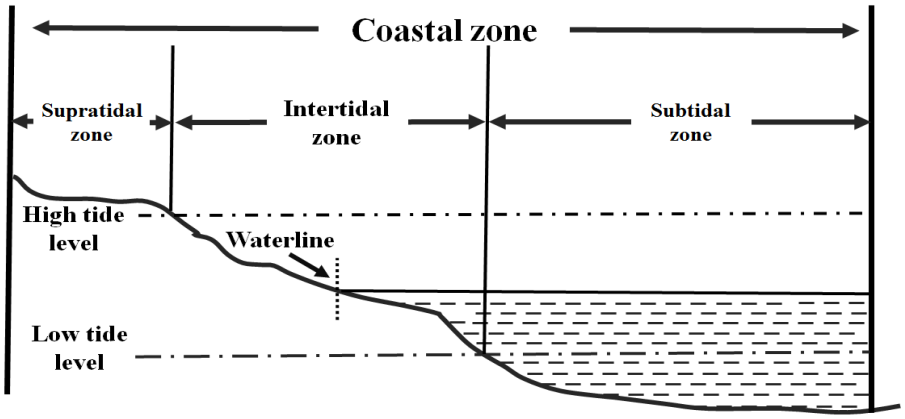

Figure 1-1. Illustration of the coastal zone

Tidal flats are distributed widely along coastlines worldwide. Among these tidal flats such as North Sea, the west coast of Europe and the Amazon, the west coast of the Korean Peninsula is one of the famous tidal flats because of its large tidal range and vast tidal flats.

Tidal flats are highly productive areas and although biological diversity may be relatively low, tidal flats support a high biomass of micro- and infaunal organisms, support large fin and shellfish stocks and play an important role in intertidal nutrient chemistry. Tidal flats provide enormous water carrying capacity, protecting coastal areas from storm surge as well as storm water runoff. Tidal flats often form the buffer zone between deeper reaches of the lagoon thereby protecting intertidal habitats by dissipating wave energy, thus reducing erosion of mangroves and salt marshes. Altogether, tidal flat is an important coastal geomorphologic system that provides habitats for wildlife, resources for land reclamation and protection for the coast against extreme storm events (Allen, 2000; Allen and Pye, 1992; Wang et al., 1999).

Because of the above mentioned impacts, the coastal environmental changes such as morphologic or topographic changes in tidal flat have attracted world-wide interest (Van Stokkom et al., 1993; Welch et al., 1992). Therefore, continuous periodic observation of morphologic and topographic changes in long-term to understand spatio-temporal characteristics are considered necessary.

Although conventional ground surveying can achieve high accuracy of measurements and intertidal sediment distribution is a reliable method of assessing changes, these ground observations are strongly restricted by limited accessibility and short exposure time between tides. Furthermore, field data may not be spatially representative due to errors introduced through sediment sampling and subsequent interpolations (Tyler et al., 1996).

On the other hand, remote sensing has an advantage of surveying a large extent of region of interest in a short time; thus remote sensing techniques are widely used in studies of topographic changes of tidal flats. Remote sensing techniques that most commonly employed over tidal flats are airborne LiDAR (Light Detection And Ranging) (Flood and Gutelius, 1997; Stockdon et al., 2002; Deronde et al., 2006), airborne InSAR (Interferometric Synthetic Aperture Radar) (Greidanus et al., 1999; Wimmer et al., 2000). However, airborne survey can only be carried out in limited circumstances due to high cost sensor systems and non-periodic observations although LiDAR and single-pass InSAR can provide highly accurate data (Cracknell, 1999; Ryu et al., 2008). Furthermore, it is difficult to retrieve the tidal flat topography of the past few years or even decades using mentioned techniques.

Earlier, much research generates the DEM from digital aerial stereo-images based on the photogrammetric techniques, and attempt to detect the topographic changes. However, in South Korea, before the 2000, the aerial image was not digital, therefore scan the film base aerial images to the digital format were used. Therefore, in this process has a high potential to occur the uncertainty (Lee et al., 2010; Ahn et

al., 2011; Lee et al., 2011). Furthermore, aerial photo swath is too small to observe the macro-tidal flat, because the surface of tidal flat always changed by flood and ebb tide. The advantage and limitations of well-used method for generate the DEM were listed as the Table 1-1.

Table 1-1. Advantage and limitations in the generate the DEM in the tidal flats (Cracknell, 1999; Lee et al., 2010; Phinn, et al., 2000; Ryu et al., 2002; Schwabisch et al., 1997; Wimmer et al., 2000).

No.	Method	Advantage	Limitations
1	In-situ measurements	High accuracy	Limited survey area and periodic observation.
2	Ship-based observation	High accuracy	Largely dependent on bathymetry; limited accessibility at shallow area. High cost for periodic observations. Influence of weather conditions.
3	Air-borne based observation	High resolution data	High cost for large survey area. Dependent on meteorological condition.
4	Aerial photogrammetry	High resolution, minimum 2 photography can extract the DEM.	Swath is small, much error occurrence when apply the post-processing (film format data). High cost for periodic observations.

Meanwhile, waterline method is a relatively more sophisticated method of which requires a number of satellite images as well as large manpower to construct a single dataset. However, it is considered one of the most effective alternative methods to monitor and detect the topographic changes in the large area of tidal flats because the topography of tidal flats of the past, possibly decades ago, can be restored through this method, if sufficient satellite images are secured (Ahn et al., 1989; Heygster et al., 2010; Hoja et al., 2000; Mason et al., 1995; Niedermeier et al., 2005; Kim et al.,

2007; Ryu, 2003; Ryu et al., 2008; Zhao et al., 2008).

In this study, tidal topography of the western part of South Korea will be constructed using series of Landsat satellites of which have been periodically acquiring data since 1972. Using the generated topographies, spatiotemporal variations of tidal topographies between the past and present will also be analyzed quantitatively.

2. Objective of research

The objective of this thesis is to establish an efficient method to estimate the topographic changes using the remote sensing data and utilize the method to analyze long-term spatiotemporal topographic variation of tidal flats.

This thesis consists of the following chapters. In Chapter 2, the accurate estimate of topographic changes, and the quantitative seasonal topographic changes are provided using the waterline method. Chapter 3 estimates the topographic change during the 1980s to 2010s, and combines the results of the seasonal topographic change to derive the minimum topographic changes in the western coast of Korea peninsula for about 30 years. Furthermore, A total of 82 scenes of Landsat 2, 3, 4, 5, 7 and 8 images were used to extract the waterline and generate the DEM with winter and summer during the past 30 years (1980-2010) in the Gomso and Hampyeong Bay. Chapter 4 analyzes the feasibility of estimating topographic change using the SAR interferometry technique. Finally, Chapter 5 summarizes the results and discusses the strength and limitations of this thesis and future works.

Chapter 2. Estimation of Seasonal Topographic Changes using Waterline Method

1. Introduction

Recently, intensive research has been conducted on the detection and estimation of temporal topographic changes in the tidal flat using the waterline method, based on various remote sensing data. Chen and Rau (1998) computed a Digital Elevation Model (DEM) in Taiwan using waterlines recorded by SPOT satellite images, to estimate coast erosion. Ryu et al. (2008) carried out a quantitative assessment of the morphologic changes affecting the tidal flats of Gomso Bay, Korea, using the waterline method coupled with a series of satellite images and ground truth data. Choi et al. (2011) examined the topographical control of surface sedimentary facies distribution in the Southern Ganghwa tidal flat, South Korea, by employing the intertidal DEM generated by the waterline method with Landsat Enhanced Thematic Mapper Plus (ETM+) images, combined with GIS analysis. Lee et al. (2011) analyzed the anthropogenic-related changes in local sedimentation trends and morphology, using the waterline method in the Ganghwa tidal flat, South Korea.

Although these researches have applied waterline method using remote sensing data to detect topographic changes in tidal flats, but the effect of seasonal topographic variation was not considered while monitoring such topographic changes. In this study, the amount of seasonal topographic variations are quantitatively assessed by applying the waterline method, using many optical satellite images acquired in short time span and different seasons.

2. Materials and methodology

2.1 Study area

The study area is located in the southwestern coast of the Korean Peninsula, where two major tidal flats reside in Gomso Bay and Hampyeong Bay. Tidal flats in Gomso and Hampyeong Bay are classified as semi-enclosed coast tidal flat. The climate in the study area is typically characterized by hot humid summers with weak southerly winds and cool dry winters with strong winds from north under the influence of Asian monsoon. Furthermore, the seasonal precipitation pattern involves heavy rainfall during summer and the tides are primarily semi-diurnal.

Gomso Bay, a 7–9 km wide and 20 km long funnel-shaped embayment, is located in the northern part of the study area as shown in the Figure 2-1. The main tidal channel runs parallel to the northern coast, losing its identity at the bay-mouth area. The tidal flats, extending some 3–5 km, are broadly developed along the southern shoreline of the bay, with an average slope of 0.09° (Chang and Choi, 2001). The main tidal channel, with depths up to 20 m, runs west-east in the northern section of the bay, its branch meeting Jujin Stream in the southern region of the shoreline. The mean tidal range in this area is 4.34 m, with spring and neap tide as 5.90 and 2.78 m, respectively. The maximum tidal current velocities in the main channel are 1.2 and 1.5 ms-1 during flood and ebb, respectively (Chang and Choi, 1998).

Hampyeong Bay is extended from northwest–southeast, with 8.5 and 17 km of maximum width and length, respectively, as shown in the study area map (Figure 2-

1). The mouth of this Bay is deep and narrow, with a maximum depth of about 23 m, and a width of 1.5 km (Ryu, 2003). A large area of tidal flats has been developing along the side of the Bay, characterized by small sand bars and cheniers (Ryu, 2003). The mean tidal range in this region is 3.46 m, with mean neap and spring tidal ranges of 2.37 and 4.55 m, respectively (Waska and Kim, 2010). No rivers flow into the Bay, and the groundwater discharge runoff in the intertidal area is large enough to form small streams, causing thriving microphytobenthos communities (Waska and Kim, 2010).

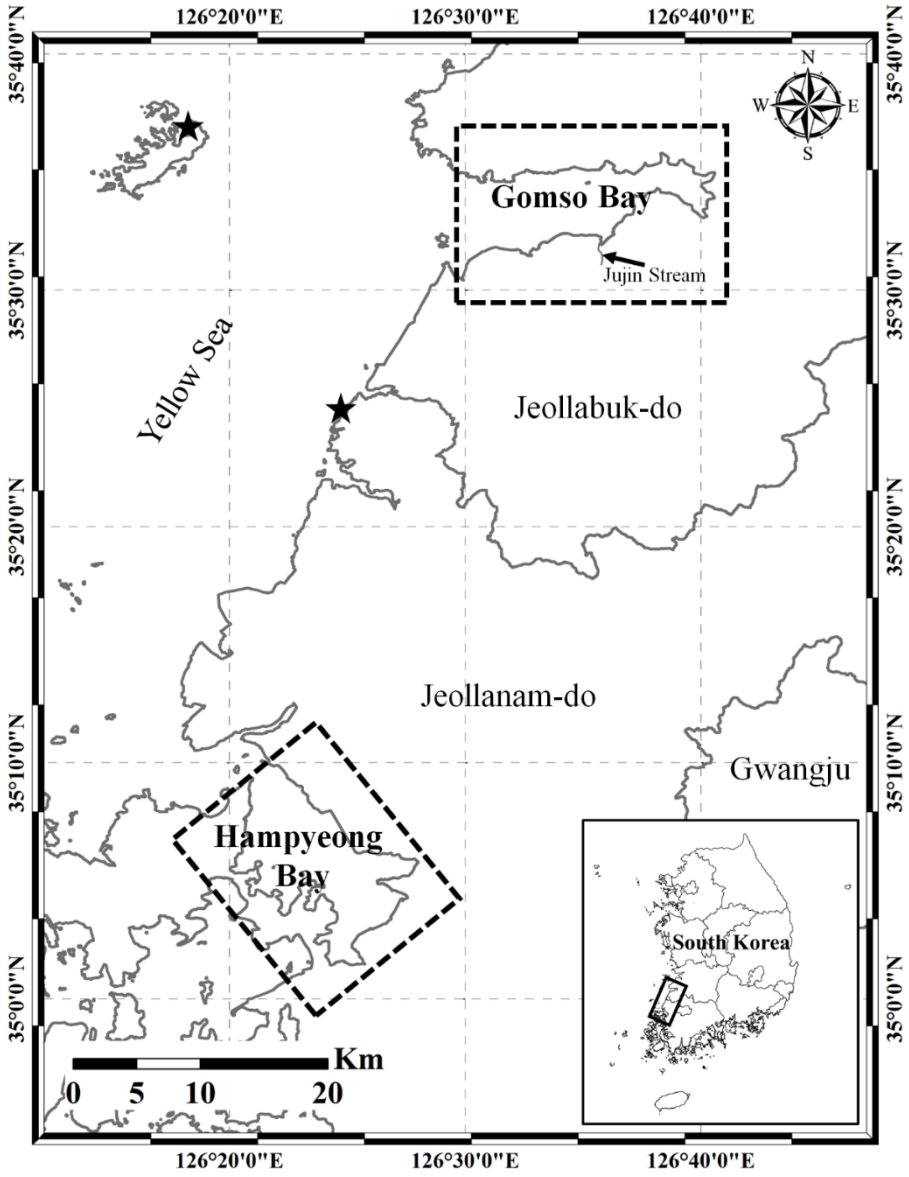

Figure 2-1. Map of the study area, including the location of Yeonggwang and Wido tidal gauge station (stars).

2.2 Remote sensing images and tidal data

Landsat TM and ETM+ data, acquired during summer (June to August) and winter (December to February) seasons, were used in our investigation. A total of 18 scenes with low-cloud effect were collected between 2003 and 2004 as listed in Table 2-1. For each bay, 9 Landsat TM or ETM+ satellite scenes, 4 in winter and 5 in summer, were chosen. In order to obtain short timespan waterline profiles, it is crucial to collect as short interval as possible for remote sensing data. For this reason, only one Landsat TM scene which was acquired in September was included unavoidably. All of the acquired images were geometrically corrected, rectified to the world geodetic survey 1984 (WGS84) datum and projected on the Universal Transverse Mercator (UTM) coordinate system.

The tidal heights used in this study are being recorded regularly by a tidal gauge at Wido and Yeonggwang station respectively located at 35°37'5'' N, 126°18'6'' E and 35°25'34'' N, 126°25'13'' E (shown as stars in Figure 2-1). The stations are operated by the Korea Hydrographic and Oceanographic Administration (KHOA), recording tidal level at one minute interval starting from November, 2001 to present, using a floating gauge. Tide ratios and mean sea levels were used to compensate for tide differences due to distances between the nearest tidal gauge station and Gomso or Hampyeong Bays on the basis of Equation (1). Corrected tidal height information is listed in Table 2-1 matching the acquisition times of acquired satellite images in each bay.

$$Corrected\ \ tidal\ \ height = (Z - Z_0) \times R + S_0 \qquad (1)$$

where, Z and Z_0 are recorded tidal height and mean sea level in the standard port (ex. Standard port of Gomso Bay is Wido tidal gauge station, and standard port of Hampyeong Bay is Yeonggwang tidal gauge station), R is tide ratio and S_0 is mean sea level in the any place where is Gomso or Hampyeong bay. The Z_0, R, and S_0 are reported by KHOA.

Table 2-1. List of satellite images used in this study. The images of Landsat TM and ETM+ were acquired during winter and summer seasons in 2003 and 2004 and corresponding tidal heights were measured at the closest tidal gauge stations.

No.	Sensor	Date	Season	Tidal height (cm)	Location
1	Landsat 5	2003-12-10	Winter	110	Gomso Bay
2	Landsat 5	2004-02-12	Winter	183	Gomso Bay
3	Landsat 7	2003-01-16	Winter	373	Gomso Bay
4	Landsat 7	2004-01-03	Winter	467	Gomso Bay
5	Landsat 5	2004-07-05	Summer	129	Gomso Bay
6	Landsat 5	2004-06-03	Summer	221	Gomso Bay
7	Landsat 7	2004-08-14	Summer	320	Gomso Bay
8	Landsat 5	2003-09-21	Summer	406	Gomso Bay
9	Landsat 7	2004-07-29	Summer	458	Gomso Bay
10	Landsat 7	2003-01-16	Winter	373	Hampyeong Bay
11	Landsat 7	2003-02-01	Winter	183	Hampyeong Bay
12	Landsat 5	2003-02-25	Winter	467	Hampyeong Bay
13	Landsat 5	2003-09-21	Summer	393	Hampyeong Bay
14	Landsat 5	2003-12-10	Winter	108	Hampyeong Bay
15	Landsat 5	2004-06-03	Summer	213	Hampyeong Bay
16	Landsat 7	2004-06-27	Summer	461	Hampyeong Bay
17	Landsat 5	2004-07-05	Summer	124	Hampyeong Bay
18	Landsat 7	2004-08-14	Summer	309	Hampyeong Bay

2.3 Methodology

In order to quantitatively estimate seasonal topographic variation in the tidal flat, waterline method is used to construct a topographic map. The term ‘waterline’ is defined as the boundary between water body and exposed tidal flat, recognizable in a remotely sensed image (Mason et al., 1997). Assuming that the waterline is a line of equal elevation, one can generate an intertidal DEM by stacking a series of waterlines observed under different tidal conditions.

There are several procedures to define the waterline from remotely sensed images, and these can be separated into two methods, namely the automatic approach, and the digitizing method through visual investigation. Due to image noise and the uncertainty associated with the extraction process, the waterlines defined by automatic methods were usually discontinuous, and further modification was required (Liu et al., 2012).

On the other hand, human eyes are generally sensitive to edges and boundaries, such as waterlines in satellite images, even though they cannot perform mathematical measurements. Additionally, rational judgment skills provide useful inputs in defining which edges are relevant (Niedermeier et al., 2005). Furthermore, On May 31, 2003, the Scan Line Corrector (SLC), which compensates for the forward motion of Landsat 7, failed (SLC-off). Because of this reason, automated waterline extraction method is hard to approach these images.

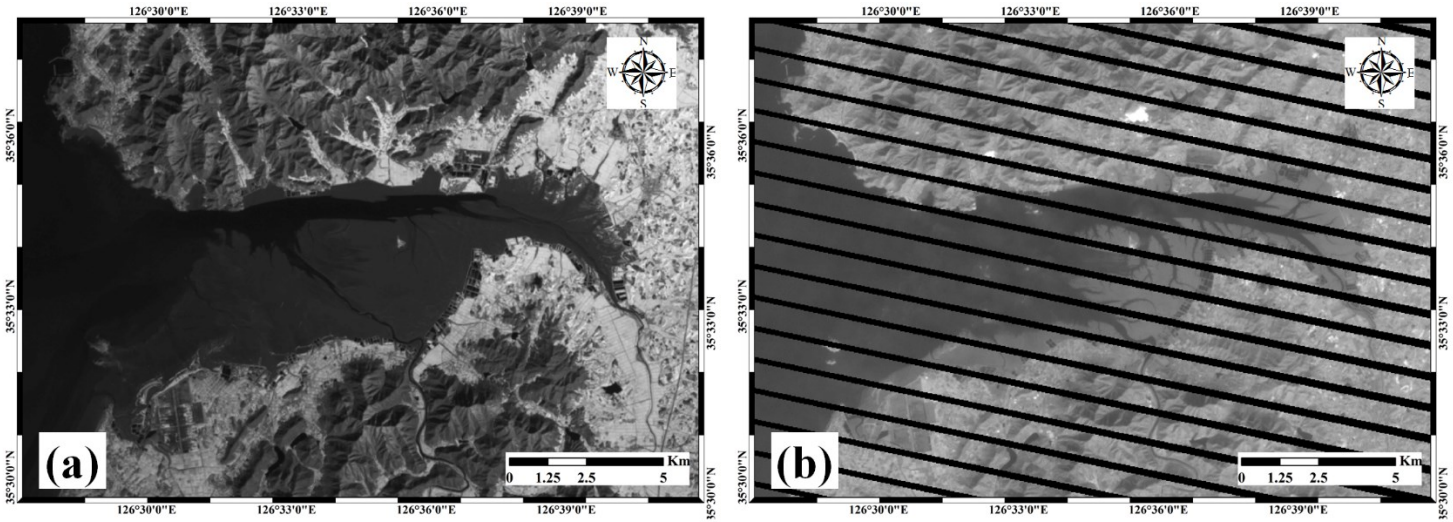

Figure 2-2. Represent of the Landsat-7 satellite images SLC on(a) and SLC off(b) mode. In the SLC off mode image, the diagonal lines were occurred. It is hard to extract the waterlines by the automated method.

Therefore, the digitizing method through visual investigation is an effective and straight-forward procedure, here employed to obtain accurate and reliable waterlines. In this study, the (Near Infra-Red) NIR band mainly used, and natural color image and combination of NIR, Green, Blue band were accessory used to conform the correct waterline. Furthermore, digitizing by visual investigation is an unique method to extract the waterlines from Landsat -7 SLC-off images. Since the diagonal lines are uniformly spaced and follows same pattern, the extraction of waterlines is similar to SLC-on image and more importantly the expected error is not significant when compared to SLC-on images.

Using this approach, a series of waterlines of each season were extracted from the satellite images. Then, the summer and winter seasons DEMs (S_DEM and W_DEM, respectively) were generated using the Natural Neighbor interpolation algorithm (Sibson, 1981), based on the extracted summer and winter waterlines. This algorithm finds the closest subset of input samples to a query point and applies weights to them based on proportionate areas to interpolate a value. This method is also known as Sibson or "area-stealing" interpolation. Finally, the seasonal topographic changes were calculated by subtracting W_DEM from S_DEM.

In this study, the waterline method is applied to estimate the quantitative changes of seasonal variation in the tidal flat. The ‘waterline’ is defined as the boundary between a water body and an exposed tidal flat in a remotely sensed image (Mason et al., 1997). Assuming that the waterline is a line of equal elevation, one can generate an intertidal DEM by stacking a series of waterlines observed under different tidal

conditions.

In order to calculate the quantitative topographic changes of seasonal variation in the tidal flat, the waterlines of each season are extracted from the selected satellite images. Then, the summer season DEM (S_DEM hereafter) and winter season DEM (W_DEM hereafter) were generated using the Natural Neighbor interpolation algorithm based on the extracted summer and winter waterlines, respectively. The Natural Neighbor interpolation algorithm finds the closest subset of input samples to a query point and applies weights to them based on proportionate areas to interpolate a value (Sibson, 1981). It is also known as Sibson or "area-stealing" interpolation. At last, the topographic change of seasonal variations is calculated by subtracting W_DEM from S_DEM.

2.4 Error estimation

The error estimation processes of the topographic changes by the waterline method using remote sensing data following the flowchart (Figure 2-3). First of all, the waterline extraction was performed which using the automated method and the digitizing through visual investigation method. For the objective assessment of the extracted waterline that from digitizing though visual investigation, the waterline extracted by the Supposed Vector Machine(SVM) used for reference waterline to comparison of the SVM_waterline and Digitized_waterline. And then, convert the Digitized_waterline to the vertexes, and calculate the distance between the vertex to

the nearest point of the SVM_waterline. At last, aspect of tidal flat was included to estimate the error which using the waterline method to estimate the seasonal topographic changes.

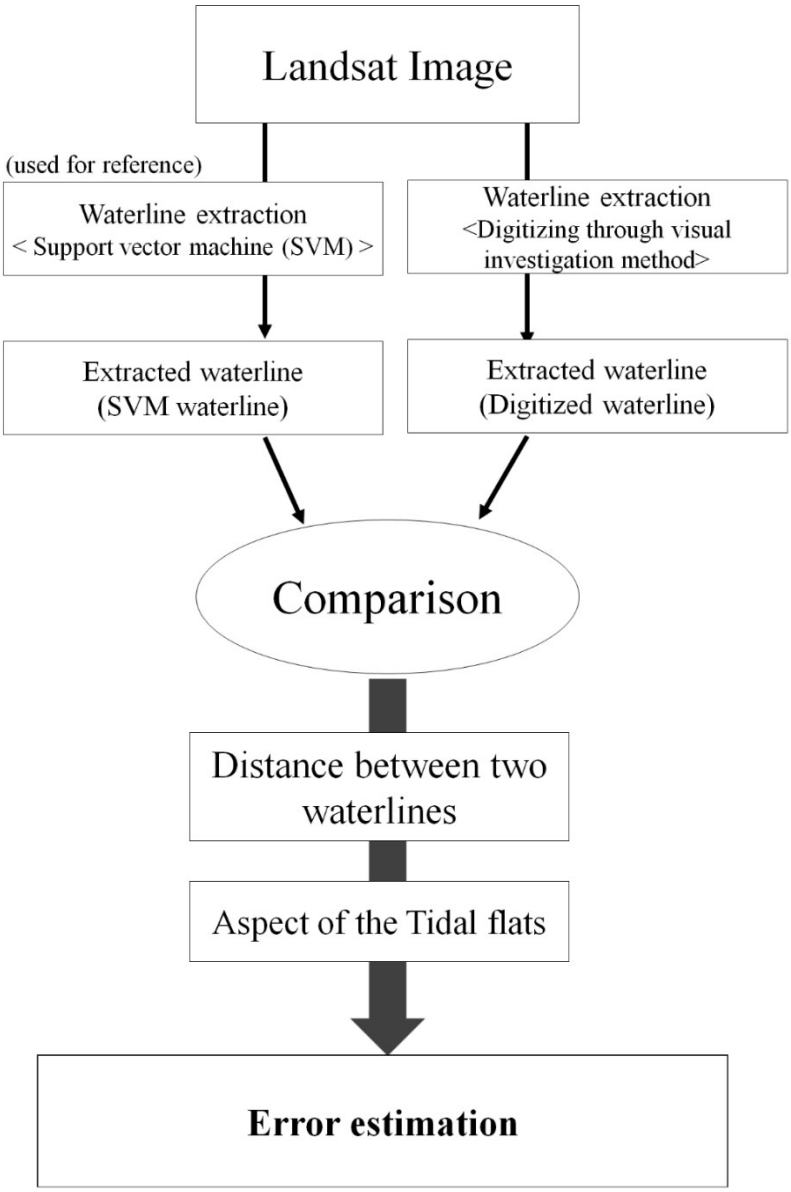

Figure 2-3. Flowchart of the error estimation.

3. Results and discussion

The error estimation was performed due to the comparison of SVM_waterline and Digitized_waterline. Figure 2-4(a) represents the result of the classification results by the SVM method in the Gomso Bay. Figure 2-4(b) shows the waterline comparison that were SVM_waterline(blue) and red colored line represents the Digitized_waterline.

Figure 2-5 also represents the result of the classification using the SVM method and waterlines comparison which extracted from SVM method and digitizing through the visual investigation, in the Hampyeong Bay.

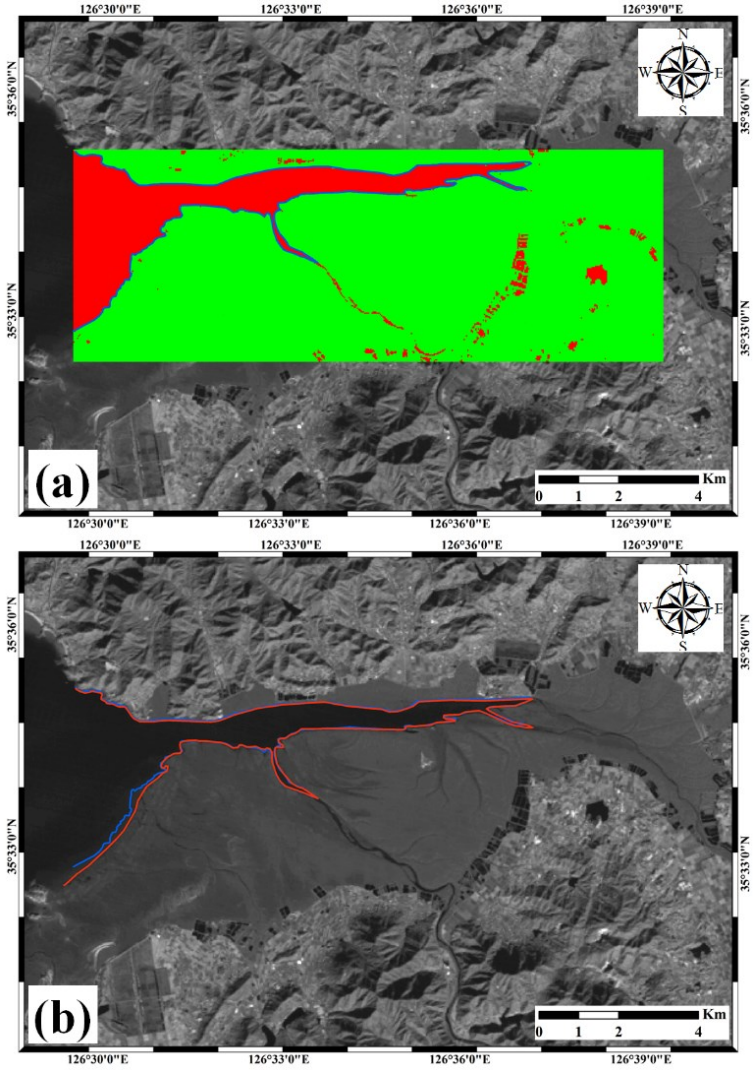

Figure 2-4. Classification results using the SVM method (a). Comparison of SVM waterline (blue), and Digitized_waterline (red) in the Gomso Bay (b).

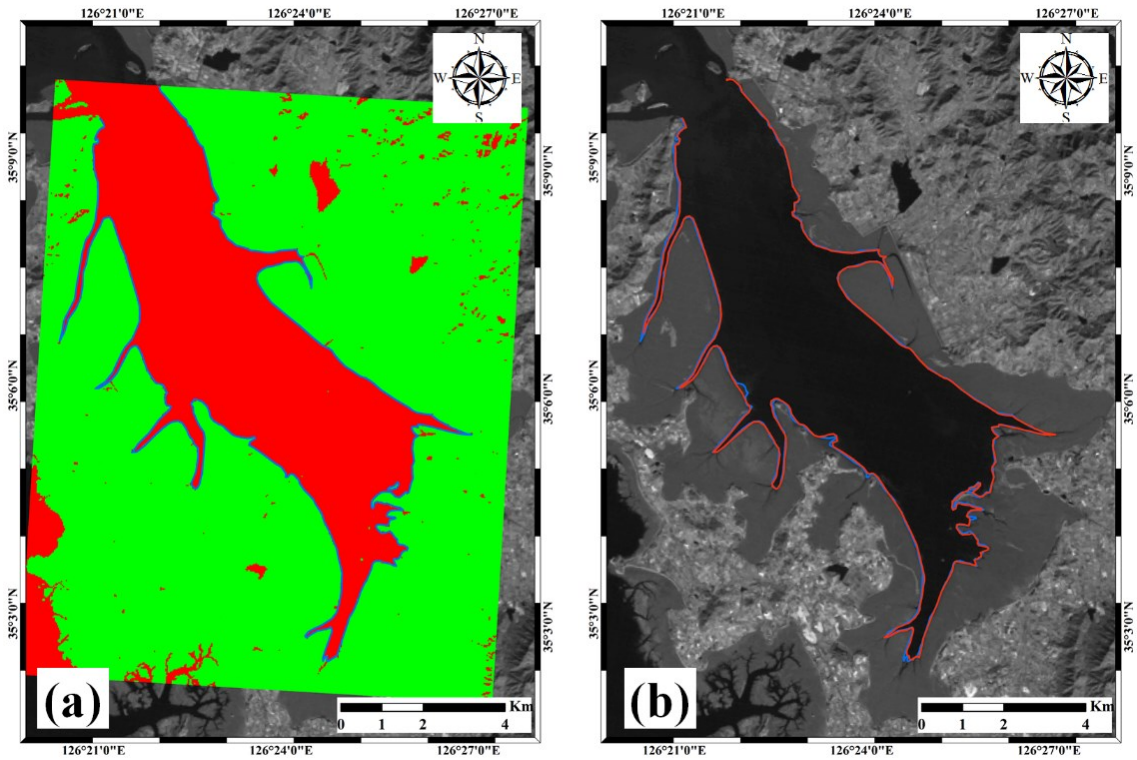

Figure 2-5. Classification results using the SVM method (a). Comparison of SVM waterline (blue), and Digitized_waterline (red) in the Hampyeong Bay (b).

Figure 2-6 and 2-7 are histogram of the waterline comparison, which using SVM method and Digitizing through visual investigation. As the results, the overall mean distance was 34.4 m, in the Gomso Bay. Also, the mean distance was calculated in the Hampyeong bay with 21.5 m. As the results, the overall mean distance were about 30m, it is similar to the spatial resolution of the used Landsat data.

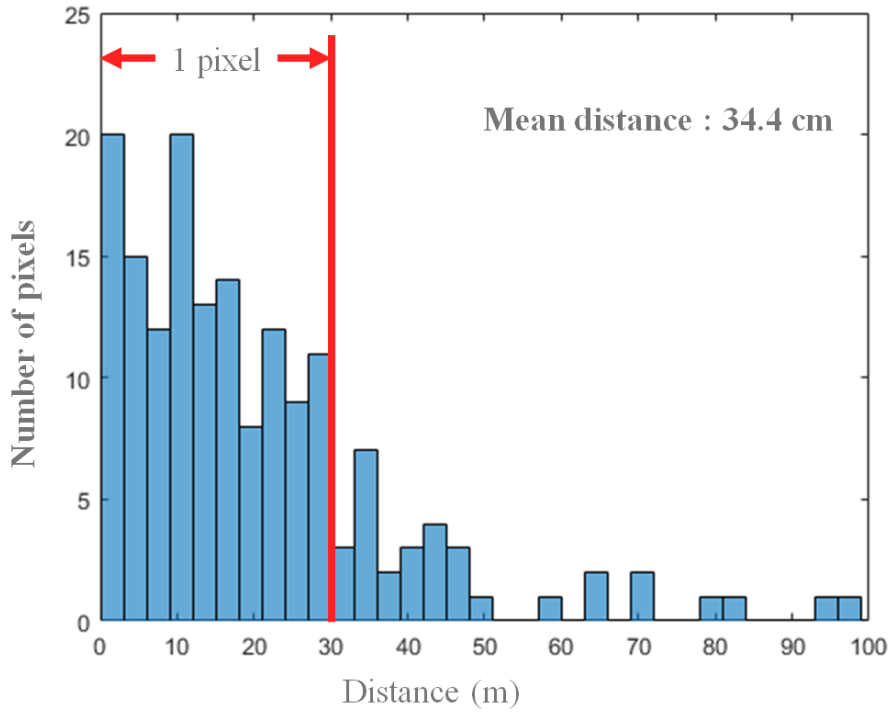

Figure 2-6. Histogram of the waterline comparison results in the Gomso Bay.

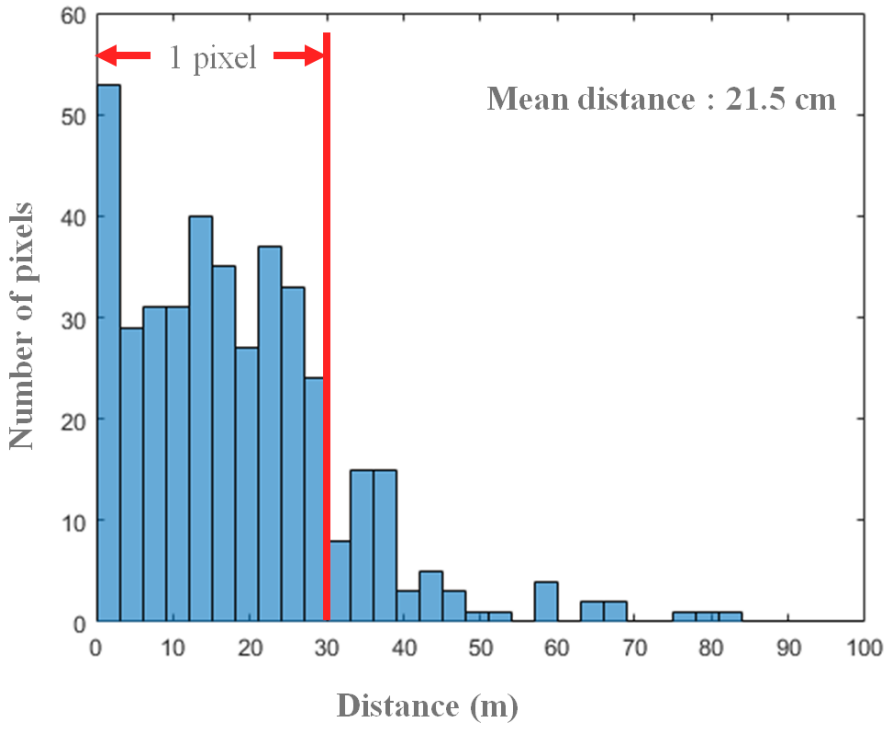

Figure 2-7. Histogram of the waterline comparison results in the Hampyeong Bay.

At last, the aspect information of the Gomso and Hampyeong Bay were included to estimate the error. In the previous study (Jang et al., 1998; Ryu 2003), the aspect were 0.09º and 0.06º, respectively, in Gomso and Hampyeong Bay. Therefore, the results of vertical height error were 5.4 cm and 2.3 cm, in the Gomso and Hmapyeong bay, respectively.

Figure 2-8 represents the extracted waterlines and DEMs of the tidal flats in Gomso (Figure 2-8 a and b) and Hampyeong bay (Figure 2-8 c and d) by the digitizing through visual investigation method. The DEMs are overlaid by the waterlines during winter and summer seasons drawn in blue and red gradient colors, respectively. The background image corresponds to the NIR band of the Landsat TM satellite image, acquired on 10th December, 2003, when the tidal height was around 110 cm. The waterlines in Gomso Bay represent tidal heights ranging from 110 to 456 and 129 to 458 cm during winter and summer season, respectively, as shown in Figure 2-8(a) and (b). Similarly, the waterlines in Hampyeong Bay represent tidal heights ranging from 108 cm to 467 cm and 124 cm to 461 cm during winter and summer season, respectively as shown in Figure 2-7c and d. The DEMs were interpolated with a spatial resolution of 0.3 m and the boundary conditions, the maximum and minimum height of the interpolation, were employed from the height ranges of each season. Then, the maximum and minimum heights of both W_DEM and S_DEM were bounded from 129 cm to 456 cm and 124 cm to 467 cm, respectively, to rule out the amount difference caused by the extent mismatch in Gomso and Hampyeong Bay.

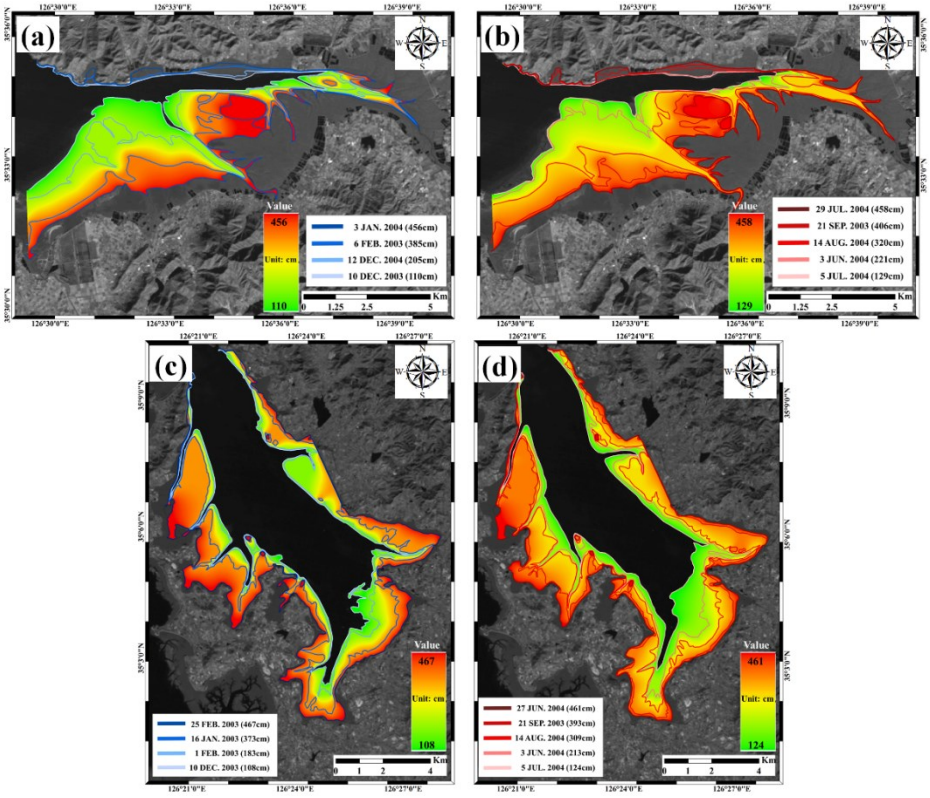

Figure 2-8. Generated DEMs of winter and summer seasons overlaid by the extracted waterlines represented in winter (blue solid lines) and summer (red solid lines) in Gomso(a,b) and Hampyeong(c,d) Bay, respectively. (a) W_DEM of Gomso bay; (b) S_DEM of Gomso Bay; (c) W_DEM of Hampyeong bay and (d) S_DEM of Hampyeong bay.

The accuracy of a DEM yielded by the waterline method largely depends on the accuracy of the waterlines. The average length of the extracted waterlines was about 51,785 m and 66,954 m slightly varying depending on tidal heights; the average number of vertices to establish a single waterline was approximately 387 and 581 corresponding to one vertex for every 4 pixels (Table 2-2, 2-3).

Table 2-2. Detailed information about the extracted waterlines in Gomso Bay. The length of each waterline slightly varies depending on the tidal height of the acquisition date.

No.	Date	Tidal height (cm)	Location	Waterline length (m)	Vertices	length per vertex (m)
1	2003. 01. 16	373	Gomso Bay	54930	442	124
2	2003. 09. 21	406	Gomso Bay	77207	708	109
3	2003. 12. 10	110	Gomso Bay	33523	173	194
4	2004. 01. 03	467	Gomso Bay	65075	447	146
5	2004. 02. 12	183	Gomso Bay	52264	388	135
6	2004. 06. 03	221	Gomso Bay	36339	310	117
7	2004. 07. 05	129	Gomso Bay	27084	115	236
8	2004. 07. 29	458	Gomso Bay	70032	669	105
9	2004. 08. 14	320	Gomso Bay	49612	230	216
Average				**51785**	**387**	**134**

Table 2-3. Detailed information about the extracted waterlines in Hampyeong Bay. The length of each waterline slightly varies depending on the tidal height of the acquisition date.

No.	Date	Tidal height (cm)	Location	Waterline length (m)	Vertices	length per vertex (m)
1	2003. 01. 16	373	Hampyeong Bay	79716	787	101
2	2003. 02. 01	183	Hampyeong Bay	65987	574	115
3	2003. 02. 25	467	Hampyeong Bay	69872	744	94
4	2003. 09. 21	393	Hampyeong Bay	74133	732	101
5	2003. 12. 10	108	Hampyeong Bay	62208	406	153
6	2004. 06. 03	213	Hampyeong Bay	67429	489	138
7	2004. 06. 27	461	Hampyeong Bay	63207	508	124
8	2004. 07. 05	124	Hampyeong Bay	45292	308	147
9	2004. 08. 14	309	Hampyeong Bay	74741	683	109
		Average		**66954**	**581**	**115**

The seasonal topographic variations, i.e., DEM_S minus DEM_W, are shown in Figure 2-9 where red and green color represents summer deposition and summer erosion. In this study, summer deposition means that the surface height of summer season is relatively higher (relatively deposited) than that of winter season, while summer erosion represents that the surface height of summer season is relatively lower (relatively eroded) than that of winter season.

For comparison of spatial patterns in Gomso and Hampyeong Bay, the study areas were split into outer, middle and inner part. This separation considers the direction of the formation and the length of bays (Figure 2-9 a and b). The interval between sections was ~6 km, each was defined as Gomso_1 (outer), 2 (middle) and 3 (inner) in Gomso Bay (Figure 2-9a) whereas the interval of Hampyeong Bay was ~5 km. These were labeled as Hampyeong_1 (outer), Hampyeong_2 (middle) and Hampyeong_3 (inner) (Figure 2-9b).

In Gomso Bay, summer deposition was observed moving away from the offshore whereas summer erosion was spatially distributed around the landward direction near the offshore. In overall, the average seasonal topographic variation of the entire bay illustrates that summer deposition was dominant in winter during 2003-2004 year (Table 2-4). The largest summer deposition was observed in the outer part (Gomso_1) with 32.2 cm; relatively smaller summer deposition was observed in the middle (Gomso_2) and inner (Gomso_3) part of the bay with the average topographic changes of 5.1 and 18.5 cm, respectively.

In Hampyeong Bay, summer deposition was distributed around the main tidal channels. The summer erosion was mainly observed onshore of the most parts of Hampyeong Bay. The spatial average of each section of Hampyeong Bay is listed in the lower part of Table 2-4. The average seasonal topographic change of Hampyeong_1 was around 1.5 cm representing summer deposition. On the other hand, summer erosion was dominant with the topographic changes of -9.3 cm and -7.2 cm in the middle (Hampyeong_2) and the inner (Hampyeong_3) segment of the bay, respectively.

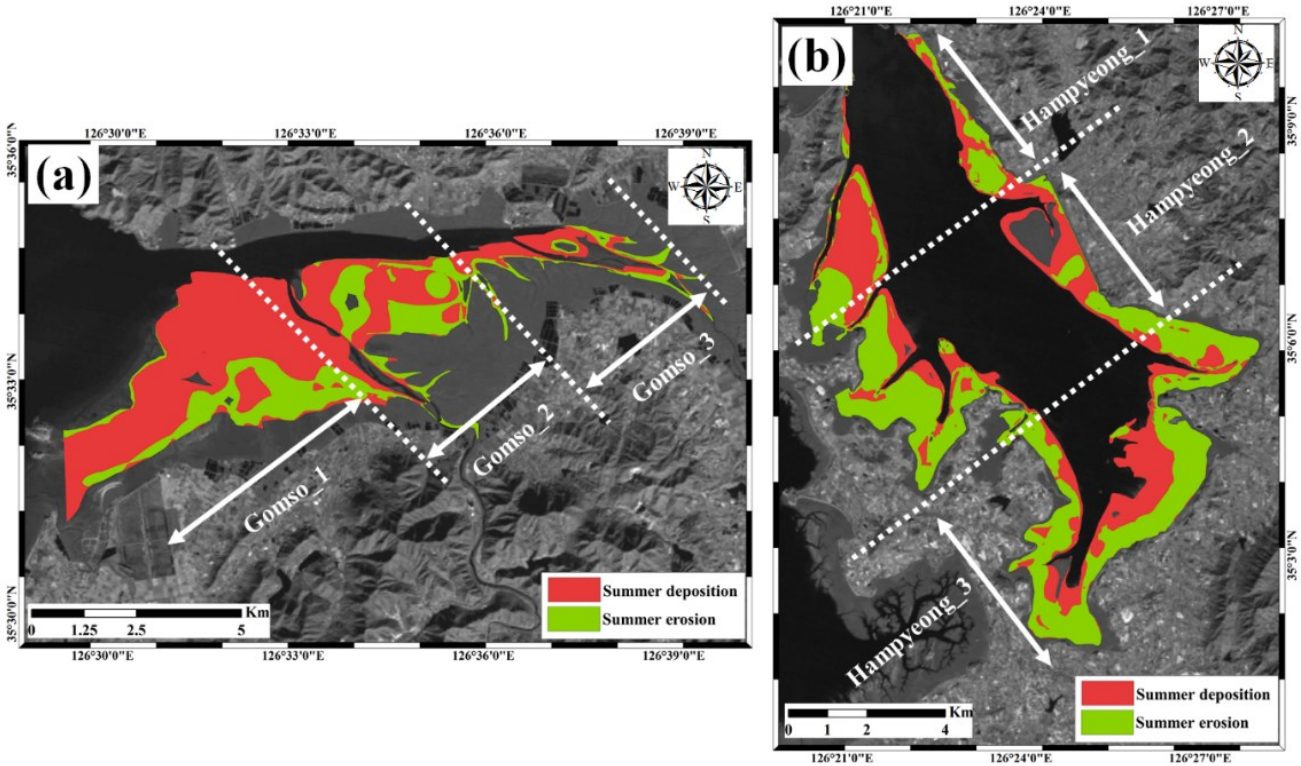

Figure 2-9. Spatial distributions of summer deposition and erosion are shown in red and green, respectively. The entire bays are split into 3 sections according to the length and formation shape of each bay. (a) Gomso Bay; (b) Hampyeong Bay. In this study, summer deposition means that the surface height of summer season is relatively higher (relatively deposited) than that of winter season, while summer erosion represents that the surface height of summer season is relatively lower (relatively eroded) than that of winter season.

Table 2-4. Quantitative seasonal topographic changes in Gomso and Hampyeong Bay. The average variation of each section is also listed.

Bay	Seasonal topographic variation(cm)	Overall average seasonal topographic variation(cm)
Gomso_1	32.2	
Gomso_2	5.1	**18.6**
Gomso_3	18.5	
Hampyeong_1	1.5	
Hampyeong_2	-9.3	**-5.0**
Hampyeong_3	-7.2	

Figure 2-10 shows the quantitative topographic variation in Gomso and Hampyeong Bay. The maximum variation (summer deposition) was spotted in the entrance area in Gomso Bay; the largest summer erosion was observed in the middle and inner part. In Hampyeong Bay, the largest summer deposition was located around the inner southern part of the bay where summer erosion also showed the strong signal in north. The main cause of these local maximum topographic variations are suspected to be the migration of tidal creeks and that main tidal creeks are developed inside bays.

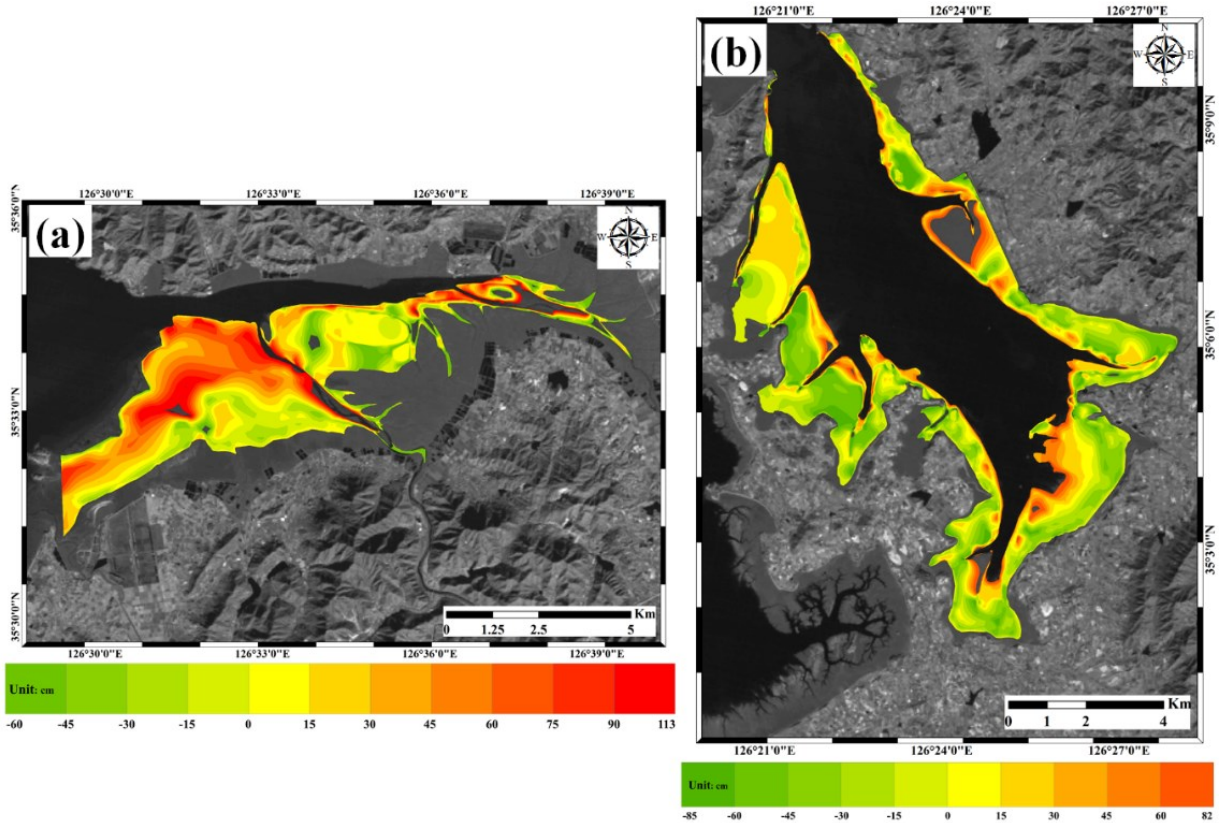

Figure 2-10. Quantitative seasonal topographic variations of (a) Gomso Bay and (b) Hampyeong Bay. The maximum summer deposition was spotted near the entrance of Gomso Bay while the largest summer erosion was observed in the middle and inner part. In Hampyeong Bay, the largest summer deposition was located around the inner southern part of the bay.

The overall average topographic variation of tidal flats in Gomso and Hampyeong Bay was about 18.6 cm and -0.5 cm, respectively. Although Gomso and Hampyeong Bay consist of semi-enclosed tidal flats, the seasonal topographic variation in each bay was different during 2003-2004 season; summer deposition was dominant in Gomso Bay whereas summer erosion was dominant in Hampyeong Bay. These results are consistent with previous studies providing field measurements (Alexander et al., 1991; Ryu et al., 1999; Ryu, 2003). Possible sources for this difference are considered to reside in the formation shape and sediment type of the tidal flats. Concerning the formation shape, the tidal flat in the Hampyeong Bay was developed along north-west and south-east directions with a narrow bay mouth. In contrast, the tidal flat in Gomso Bay was developed along the east-west direction with a wide bay entrance. In general, the monsoon is directly associated with wind direction of which blows from the north-west in the winter of the Korea Peninsula. Hampyeong and Gomso Bay have different formation shapes with different directions so that each has divergent influence from the monsoon. The erosion is relatively weaker in Hampyeong Bay of which the south-west main tidal channel diminishes the most of wave energy coming from the north-west and is connected to the bay-mouth of less than 2 km wide. On the other hand, the mouth of Gomso Bay is open towards the west with the width of about 9 km. This relatively large bay-mouth with the right direction is easily exposed to the waves from the north-west direction, influenced by the monsoon, causing the dominant erosion effect. Thus, it was analyzed that the morphology and direction of the bays have strong relation with the monsoon. In this regard, wave, typhoon, and storm events exert comparatively larger

influences on the Gomso, whereas Hampyeong Bay is well protected from those.

Tidal currents are generally the predominant sedimentary forcing agents in semi-enclosed bay environments, yielding extensive muddy tidal flats with limited sand bar formation, and a typical trend of seawards grain-size coarsening (Alexander et al., 1991; Frey et al., 1989; Postma, 1961; Van Straaten and Kuenen, 1957; Wells et al., 1990). However, Hampyeong Bay rarely follows these characteristics since the bay includes well-developed mixed flats, mud flats and sandy bodies, such as sand bars and cheniers. This unusual seasonal sedimentary pattern in Hampyeong Bay is not only controlled by tidal currents, but also by other factors such as monsoon storms and bay morphology.

In this study, the seasonal topographic variations were extracted from waterlines obtained in summer and winter season only. The topography changes was mainly influenced by the tidal current and wind directions. In general, the wind direction is towards the west coast of the Korean peninsula which predominantly influences the variations. The monsoon in Korean peninsula is directly associated with wind directions in winter from northwest to southeast and vice versa in summer. However, there is no specific characteristics of wind directions observed during spring and autumn. Therefore, the characteristics of seasonal variations in Gomso and Hampyeong Bay can be well represented by the DEMs generated in summer and winter than combining all the four seasons.

4. Summary

The seasonal topographic variation of major tidal flats in the southern part of the west sea of South Korea were quantitatively estimated by comparing the seasonal topographic differences between summer and winter DEMs derived from the waterline method. These comparisons conclude that summer deposition is the dominant effect in Gomso tidal flats with an average overall seasonal topographic change of 12.8 cm. In contrast, summer erosion is dominant with -5.0 cm topographic variation in Hampyeong Bay. Although both Gomso and Hampyeong Bay are classified as semi-enclosed coast tidal flat, the sedimentary facies caused by formation geometry and sediment type led to different topographic changes.

In comparison to previous studies, our quantitative results successfully justified the DEM generation of tidal flats, using the waterline method. In particular, the effective detection of seasonal topographic changes in the western coast of South Korea stresses the significance of this study. However, errors from multi-temporal waterlines and dimensional interpolation must also be taken into consideration in further analysis. Moreover, influential oceanic forces that can have significant influence on sedimentological processes, such as tidal currents, waves, storms, and typhoons, are expected to provide useful information on short-term topographic variations.

Chapter 3. Estimation of Topographic change from 1980s to 2010s

1. Introduction

West coast of the Korean Peninsula is famous for its large tidal range (up to 9 m) and vast tidal flats (Yoo et al., 2005). Frequent monitoring is required to protect this valuable and vulnerable ecological system, which is endangered by shipping, fishery, and tourism. However, morphologic or topographic changes in tidal flat are difficult to estimate due to the poor accessibility, short exposure and lack of suitable transportation (Ryu et al., 2008). Furthermore, it is more difficult to retrieve the tidal flat topography of the past few years or even decades by using ground surveys, ship-based echo-sounding, airborne stereo-photogrammetry (Klemas, 2011; Mason et al., 2000; Sallenger et al., 2003; Wimmer et al., 2000).

On the other hand, waterline method is relatively more sophisticated, however it is an effective alternative method to monitor and detect the topographic changes in the large area of tidal flats (Ahn et al., 1989; Heygster et al., 2010; Hoja et al., 2000; Mason et al., 1995; Ryu, 2003; Zhao et al., 2008). Furthermore, the topography of the past can be restored through the waterline method if the satellite images of the past are available; and finally, topographic evolution can be effectively monitored by comparing the generated topography.

Among the Landsat satellite series, Landsat 1 was launched in 1972 and the latest satellite, Landsat 8, was launched in 2013 operating along with Landsat 7 periodically observing the surface of Earth. The satellites orbit at 905 km above the surface with a cycle at every 103 minutes, 14 cycles a day and complete coverage of Earth every 18 days.

In this chapter, we acquire Landsat images during the 1980s and 2010s, and apply the waterline method to generate DEMs of the major tidal flats in the southern part of West Sea of the Korean Peninsula representing each period. As described in the previous chapter, the seasonal topographic variation is also taken into consideration to accurately analyze the long-term variation. Furthermore, the temporal topographic variance was performed during the 1980s to 2010s, in the Gomso and Hampyeong Bay.

2. Materials and Methodology

2.1 Remote sensing images and tidal data

In this chapter, a total of 82 scenes of low-cloud effect Landsat images were used to generate DEMS of 1980s to 2010s in Gomso and Hampyeong Bay as listed in Table 3-1 and 3-2. All of the acquired satellite images were geometrically corrected and rectified to the world geodetic survey 1984 (WGS84) datum and projected on the Universal Transverse Mercator (UTM) coordinate system using the second-order polynomial geocoding model with the nearest neighbor resampling method.

In Gomso Bay, a total of 42 scenes Landsat images were used to generate the DEM in each decade, used Landsat images were acquired during the 1980s to 2010s (Table 3-1). In the 1980s, a total of 11 scenes of Landsat 2, 3, 4 and 5 images were used to generated the 1980s DEM. In the 1990s, a total of 11 scenes of Landsat images were used to generate the 1990s DEM, and a total of 9 scenes of Landsat images were used to generate the 2000s DEM. For the 2010s, 11 scenes of Landsat 7 and 8 data were acquired during the winter and summer Generally, detect the topographic changes in the tidal flat using the waterline method, the spring tide and flood tide is the best tide condition, due to de exposed tidal flat area and low moisture content. Although the maximum amount of effort to set the best data, it is practically hard to collect the best tide condition data, caused by long time range (30 years) and set the same low and high tide height.

Table 3-1. List of satellite images and tide gauge data used in create 1980s DEM in Gomso Bay

No.	Sensor	Date	Season	Tidal condition	Tidal height (cm)
1	Landsat 3	1980-01-11	Winter	flood	377
2	Landsat 3	1980-02-16	Winter	flood	89
3	Landsat 2	1981-07-31	Summer	flood	155
4	Landsat 2	1981-12-04	Winter	flood	301
5	Landsat 4	1983-01-25	Winter	flood	476
6	Landsat 4	1983-03-14	Winter	flood	149
7	Landsat 4	1983-06-02	Summer	ebb	314
8	Landsat 4	1984-06-04	Summer	ebb	241
9	Landsat 5	1984-07-30	Summer	ebb	69
10	Landsat 4	1984-08-07	Summer	flood	461
11	Landsat 5	1985-06-15	Summer	flood	393
12	Landsat 4	1991-11-15	Winter	flood	371
13	Landsat 5	1992-06-18	Summer	flood	163
14	Landsat 5	1995-09-15	Summer	flood	242
15	Landsat 5	1996-06-13	Summer	Ebb	367
16	Landsat 5	1996-09-01	Summer	flood	80
17	Landsat 5	1997-03-28	Winter	flood	145
18	Landsat 5	1997-06-16	Summer	Ebb	465
19	Landsat 5	1998-03-31	Winter	flood	79
20	Landsat 5	1998-11-26	Winter	flood	248
21	Landsat 5	1998-12-28	Winter	flood	482

22	Landsat 5	1998-12-28	Winter	flood	482
23	Landsat 7	2003-01-16	Winter	flood	373
24	Landsat 5	2003-09-21	Summer	flood	406
25	Landsat 5	2003-12-10	Winter	flood	110
26	Landsat 7	2004-01-03	Winter	flood	467
27	Landsat 5	2004-02-12	Winter	flood	183
28	Landsat 5	2004-06-03	Summer	flood	221
29	Landsat 5	2004-07-05	Summer	flood	129
30	Landsat 7	2004-07-29	Summer	flood	458
31	Landsat 7	2004-08-14	Summer	flood	320
32	Landsat 7	2007-10-10	Summer	Flood	294
33	Landsat 7	2011-03-11	Winter	Ebb	197
34	Landsat 7	2012-06-17	Summer	Flood	384
35	Landsat 7	2012-12-26	Winter	Flood	364
36	Landsat 7	2013-01-11	Winter	Flood	309
37	Landsat 7	2013-02-28	Winter	Flood	46
38	Landsat 8	2013-09-16	Summer	Flood	504
39	Landsat 8	2014-01-06	Winter	Ebb	115
40	Landsat 8	2015-07-04	Winter	Flood	89
41	Landsat 7	2015-09-14	Winter	Flood	190
42	Landsat 7	2016-02-05	Winter	Flood	469

In Hampyeong Bay, a total of 40 scenes of Landsat 2, 3, 4, 5, 7 and 8 images were used to generate the DEM between 1980s to 2010s, mote detailed information about the used data were listed as Table 3-2. In 1980s, 10 scenes of Landsat images between 1980 and 1985 were used to extract the 1980s waterlines. A total of 11 scenes of Landsat images were used to generate the 1990s DEM, and a total of 9 scenes of Landsat images were used to generate the 2000s DEM. In 2010s, 7 scenes of Landsat 7 images and 3 scenes of Landsat 8 images with time duration from 2012 to 2016 were used to generate the 2010s DEM.

Table 3-2. List of satellite images and tide gauge data used for generate 1980s to 2010s DEM in Hampyeong Bay

No.	Sensor	Date	Season	Tidal condition	Tidal height (cm)
1	Landsat 3	1980-01-11	Winter	Ebb	393
2	Landsat 3	1980-02-16	Winter	Flood	90
3	Landsat 2	1981-07-31	Summer	Flood	160
4	Landsat 4	1983-01-25	Winter	Flood	496
5	Landsat 4	1983-03-14	Winter	Flood	153
6	Landsat 4	1984-06-04	Summer	Ebb	250
7	Landsat 5	1984-06-12	Summer	Flood	314
8	Landsat 5	1984-07-30	Summer	Ebb	69
9	Landsat 4	1984-08-07	Summer	Flood	481
10	Landsat 5	1985-06-15	Summer	Flood	409
11	Landsat 5	1992-01-10	Winter	Flood	140

12	Landsat 5	1993-09-09	Summer	Flood	337
13	Landsat 5	1994-07-26	Summer	Flood	139
14	Landsat 5	1996-06-13	Summer	Ebb	382
15	Landsat 5	1996-09-01	Summer	Flood	80
16	Landsat 5	1997-06-16	Summer	Ebb	485
17	Landsat 5	1998-03-15	Winter	Ebb	81
18	Landsat 5	1998-11-10	Winter	Flood	233
19	Landsat 5	1998-12-12	Winter	Flood	420
20	Landsat 5	1998-12-28	Winter	Flood	503
21	Landsat 5	1999-02-14	Winter	Ebb	308
22	Landsat 7	2003-01-16	Winter	Flood	373
23	Landsat 7	2003-02-01	Winter	Flood	183
24	Landsat 5	2003-02-25	Winter	Flood	467
25	Landsat 5	2003-09-21	Summer	Flood	393
26	Landsat 5	2003-12-10	Winter	Flood	108
27	Landsat 5	2004-06-03	Summer	Flood	213
28	Landsat 7	2004-06-27	Summer	Flood	461
29	Landsat 5	2004-07-05	Summer	Flood	124
30	Landsat 7	2004-08-14	Summer	Flood	309
31	Landsat 7	2012-06-17	Summer	Flood	372
32	Landsat 7	2012-12-26	Winter	Flood	379
33	Landsat 7	2013-01-11	Winter	Flood	318
34	Landsat 7	2013-02-28	Winter	Flood	45
35	Landsat 8	2013-09-16	Summer	Flood	488
36	Landsat 7	2014-02-15	Winter	Flood	175

37	Landsat 8	2014-07-01	Summer	Ebb	139
38	Landsat 8	2015-07-04	Summer	Flood	85
39	Landsat 7	2015-09-14	Summer	Flood	183
40	Landsat 7	2016-02-05	Winter	Flood	489

2.2 Methodology

As illustrated in flow chart (Figure 3-1), the waterlines are extracted from the acquired Landsat data for the 1980s and 2010s. The tide of each extracted waterlines is regarded as actual elevation. Then, by interpolation of the waterline at each time, a DEM of the 2010s and 1980s is generated. Finally, the 2010s DEM and 1980s DEM are subtracted to estimate the change in the intertidal terrain of 30 years. Giving to compensate for seasonal variations derived from the previous chapter, the final estimate of the change in the topography of the intertidal zone from the 2010s to 1980s is complete.

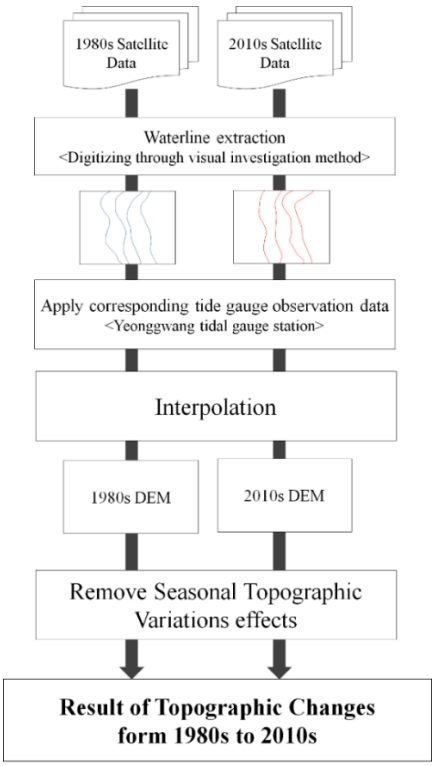

Figure 3-1. Flowchart of topographic changes from 1980s to 2010s

3. Results and discussion

3.1 Gomso Bay

Figure 3-2 (a) and (b) represents the results of waterline extraction in Gomso Bay by the digitizing through visual investigation method in the winter and summer of 1980s, represented in green and red colors, respectively. The background image is NIR band of the Landsat 8 satellite, acquired on 6th January, 2014 when the tidal height was 114 cm. Each line represents tidal heights ranging from 89 cm to 476 cm and from 69 cm to 471 cm in winter and summer during the 1980s, respectively.

Figure 3-3 represents the generated DEMs of (a) winter and (b) summer during the 2010s. The DEM was interpolated with a spatial resolution of 0.3 m and the boundary conditions, maximum and minimum height, were employed from the height ranges of each season. For the 2010s winter and summer season DEM, the tidal height ranges from 46 cm to 469 cm and from 89 to 504 cm, respectively.

Then, for quantitative estimate of the temporally topographic changes from 1980s to 2010s in the study area, the maximum and minimum heights of both DEM_1980s and DEM_2010s winter and summer are modified to same height range from 89 cm to 469 cm, and from 89 cm to 461 cm, respectively.

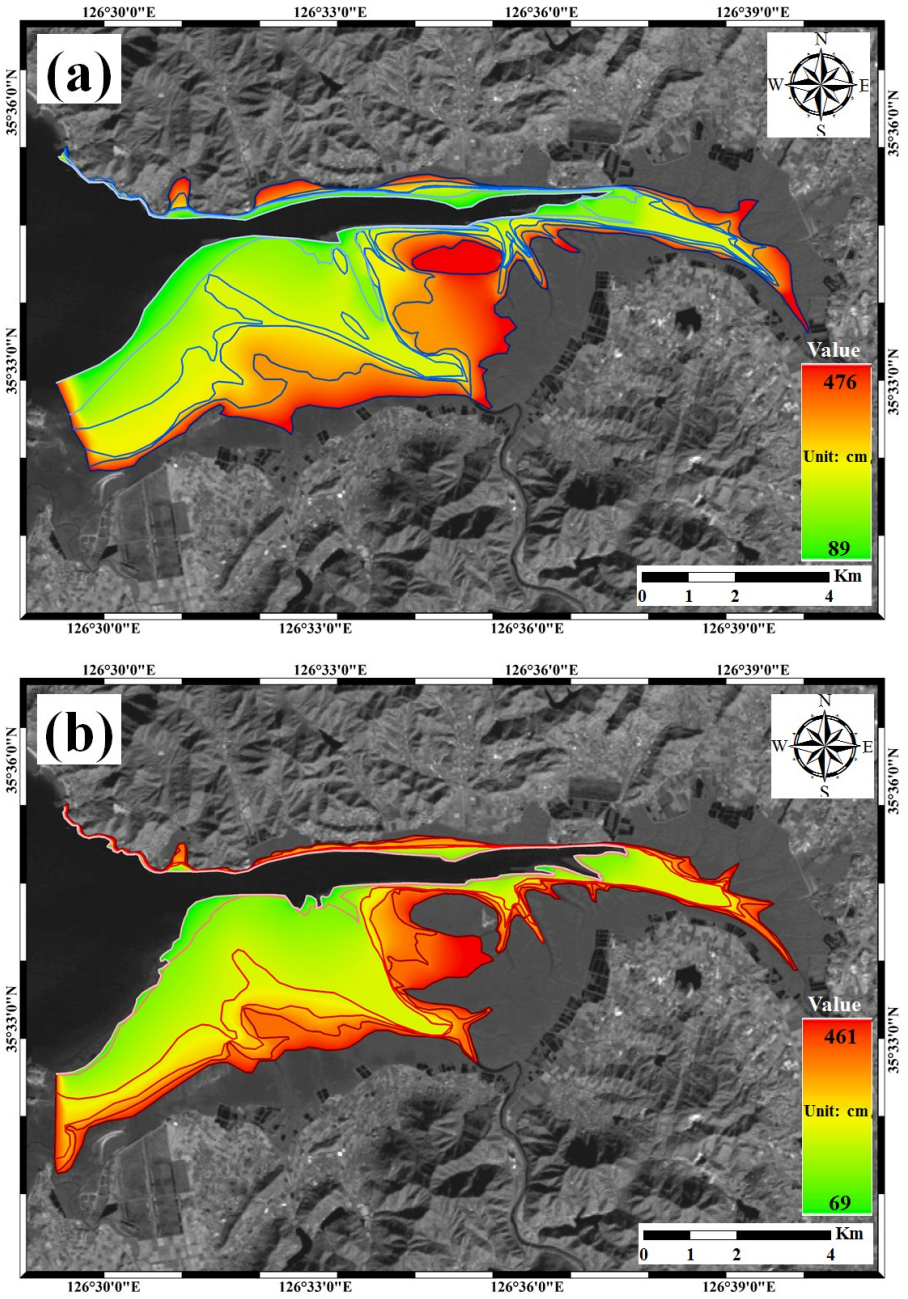

Figure 3-2. Generated DEMs for the 1980s in winter (a) and summer (b); the used waterlines are also overlaid.

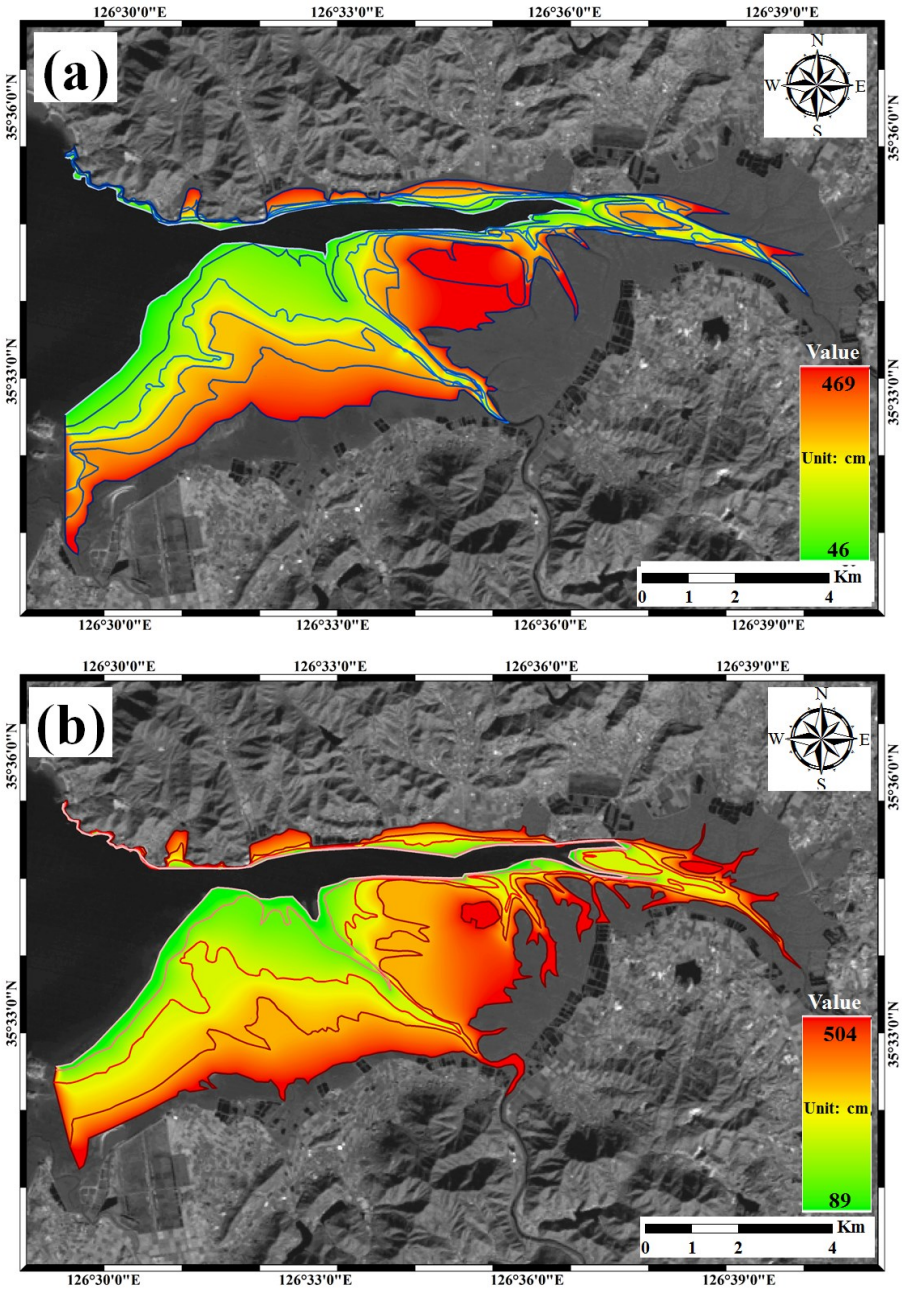

Figure 3-3. Generated DEMs for the 2010s in winter (a) and summer (b); the used waterlines are also overlaid.

Fig 3-4 and Table 3-3 show the average topographic changes in winter and summer season in Gomso Bay. According to the figure, the deposition was dominant in both summer and winter in Gomso Bay. The extent of the deposition was higher in summer than winter with about 19.5 cm.

In terms of local spatial distribution, erosion was notable near the entrance of the bay (Gomso_1) in winter; on the other hand, deposition was observed away from the bay region. In overall, deposition was dominant in most of the bay. The amount of deposition seemed to increase going into the bay entrance.

During the summer, deposition was predominant around the main tidal channels. Erosion was partially observed around the entrance and central region of the bay. Unlike winter, the direction erosion observed was towards land. These suggest that the amount of deposition was most active inside the bay and slightly decreased moving to the central region.

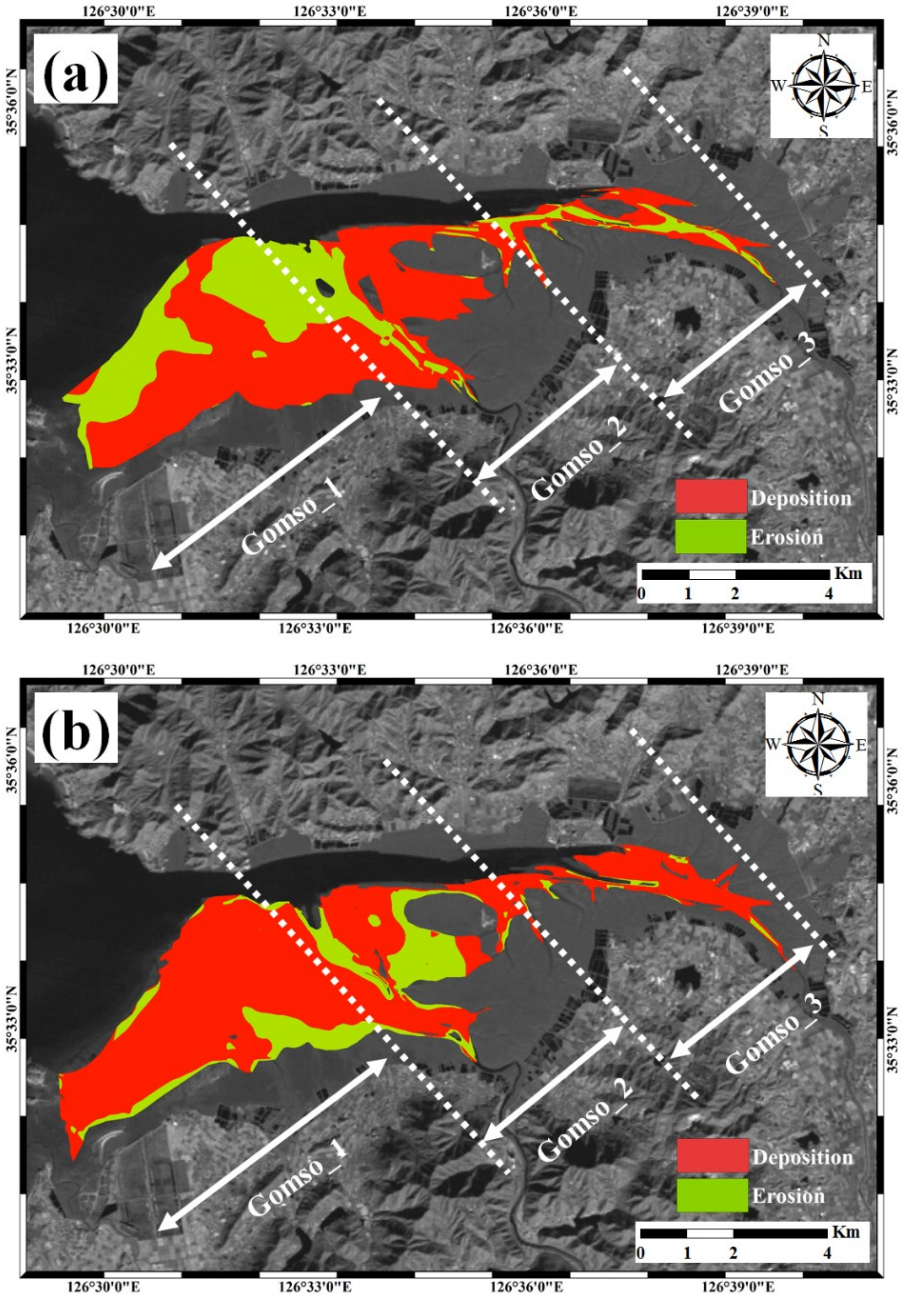

Figure 3-4. Spatial distributions of deposition and erosion are shown in red and green, respectively. The entire bays are split into 3 sections according to the length and formation shape of Gomso Bay, (a) winter; (b) summer.

Table 3-3. Spatial distribution winter and summer in Gomso Bay

Bay	Season	Average topographic variation (cm)
Gomso_1	Winter	5.2
Gomso_2		39.9
Gomso_3		47.9
Overall average topographic changes		**31.0**
Gomso_1	Summer	48.1
Gomso_2		27.9
Gomso_3		75.5
Overall average topographic changes		**50.5**

In Chapter 2, the seasonal variation of intertidal topography was estimated quantitatively. The result showed that the bay of Gomso showed a seasonal change of about 18.6 cm. Thus, this seasonal topographic variation was taken into consideration in the long term change between the 1980s and the 2010s. Figure 3-5 shows the final result of the long-term topographic since the 1980s; in the winter, deposition was about 12.4 cm and in the summer, deposition was about 31.9 cm.

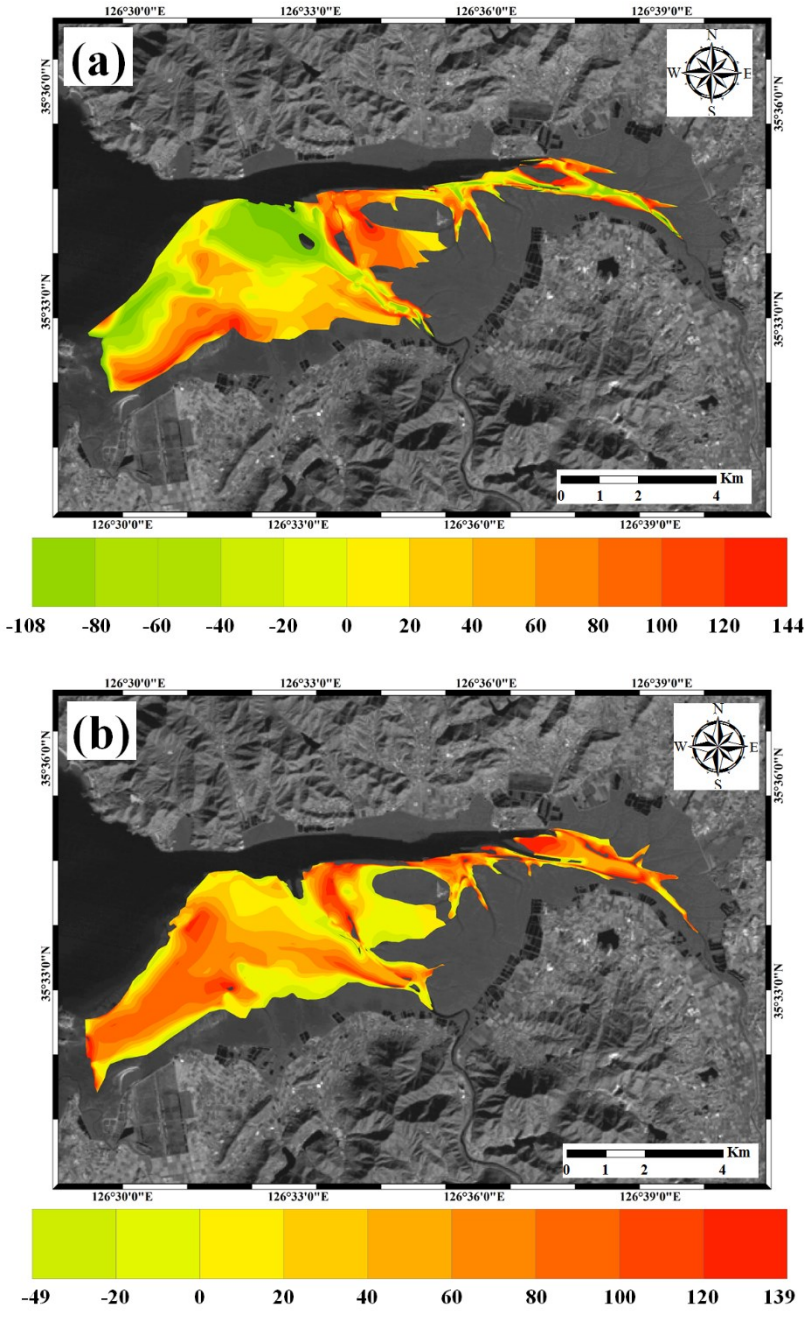

Figure 3-5. Topographic change from the 1980s to the 2010s in the winter (a) and summer (b); the seasonal variation of which was estimated in the previous chapter was taken into consideration.

The temporal topographic change was performed, during the 1980s to 2010s, in Gomso Bay. The waterline extraction and DEM were generated using the 42 scenes of the Landsat 2, 3, 4, 5, 7, and 8 satellite images (Figure 3-6 and 3-7). A total of 23 scenes of Landsat images used to extract the waterlines and generate the winter season DEMs in each decade from 1980s to 2010s (Figure 3-6). A total of 19 scenes of the Landsat images were used to extract the waterline and generate the DEMs in summer, during 1980s to 2010s (Figure 3-7). For the temporal topographic changes in the spatially, the 3 parts of regions were separated which is outer, middle, and inner part and was labeled as Gomso_1, Gomso_2, and Gomso_3, respectively.

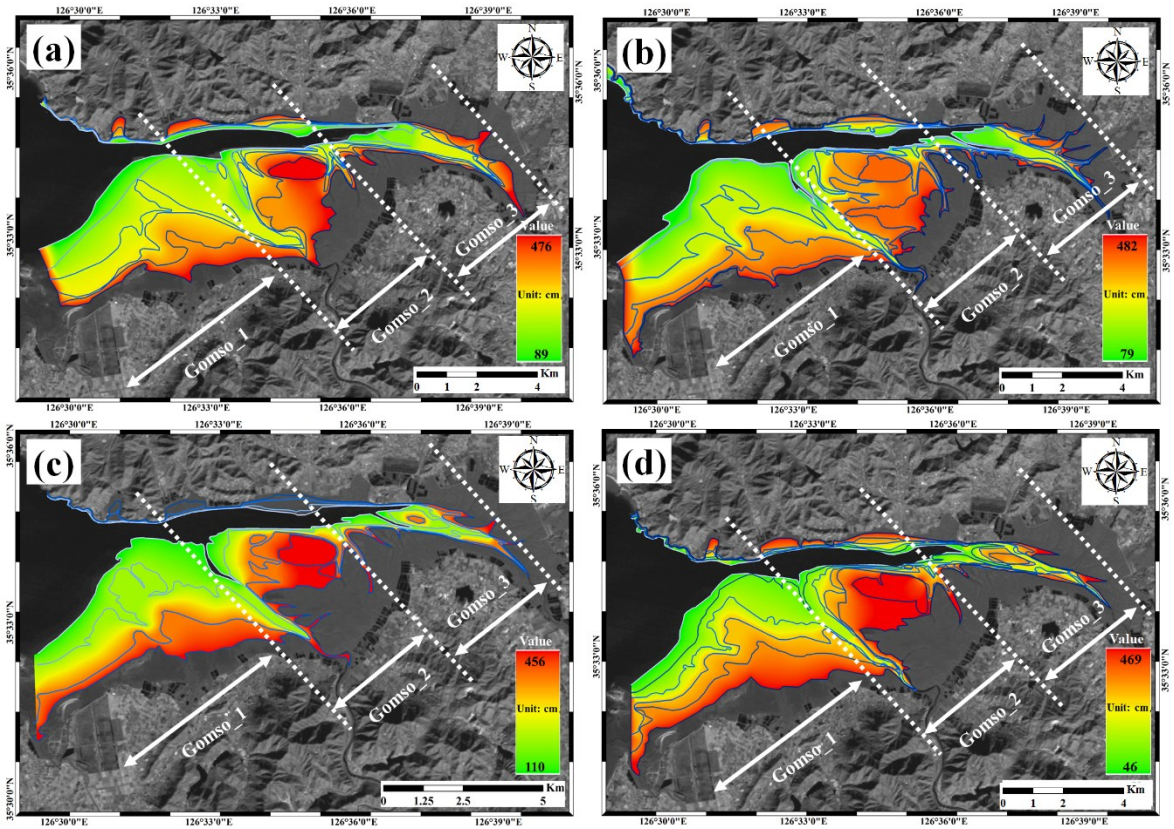

Figure 3-6. Results of waterline extraction and DEM generation using the winter season acquired Landsat images in each decade in the Hampyeong Bay, during the 1980s to 2010s. (a) 1980s; (b) 1990s; (c) 2000s; (d) 2010s

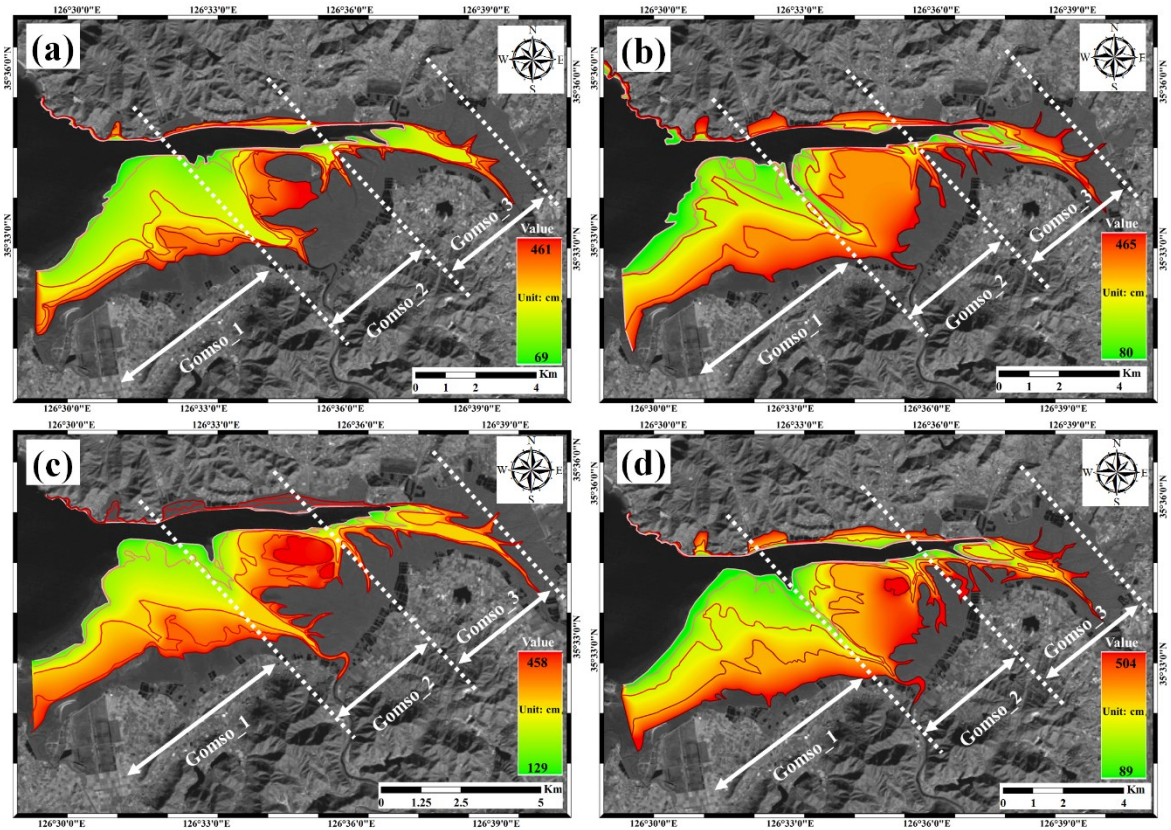

Figure 3-7. Results of waterline extraction and DEM generation using the winter season acquired Landsat images in each decade in the Hampyeong Bay, during the 1980s to 2010s. (a) 1980s; (b) 1990s; (c) 2000s; (d) 2010s

The results show the temporal changes in each part of the Gomso Bay with summer and winter season (Figure 3-8). In outer(Gomso_1) part of the Gomso bay, the deposition was dominant in summer, whereas, the erosion effect was dominant in winter season, from the past to the present. In middle (Gomso_2) part of the Gomso Bay, also the deposition was dominant in summer, and erosion was dominant in winter, from the past to the present. In the inner(Gomso_3) part of the Gomso Bay, represent the same trend of the deposition and erosion in summer and winter.

Furthermore, the results show that, as the 2000s the topographic was not regularly deposited and eroded. It might be effect on constructed big Saemangum dyke. The Saemangeum dyke, located north part of the Gomso Bay, is the world's longest man-made dyke, measuring 34 km. According to the previous study, the Saemangum dyke construction have a strong influence on the tidal current and wave directions in the neighbor areas.

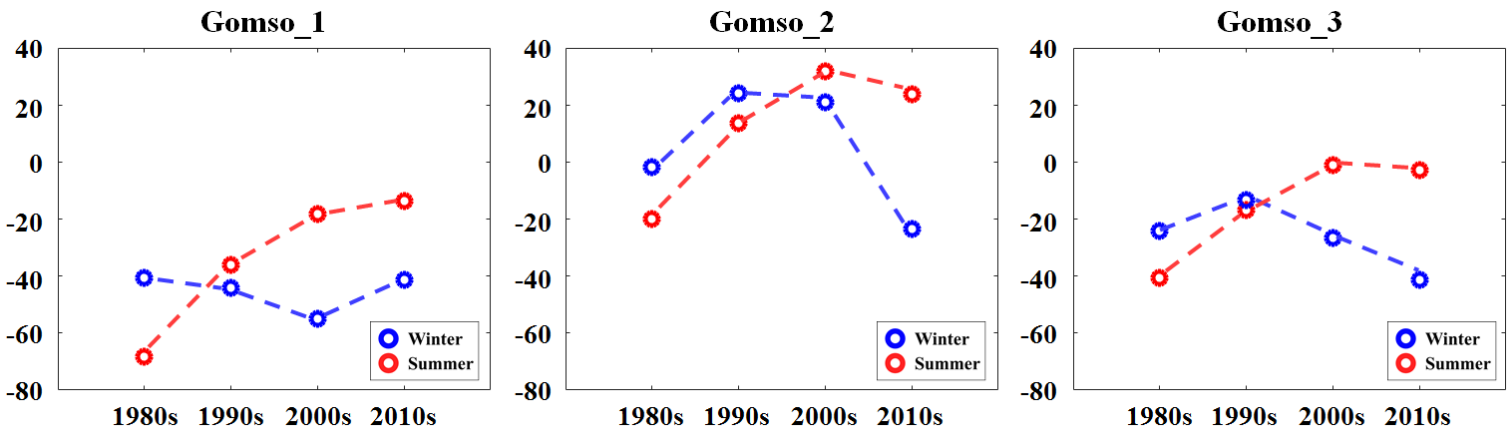

Figure 3-8. Temporal topographic changes in each part (outer, middle, and inner of the Gomso Bay) of the Gomso Bay, during 1980s to 2010s. The red cycle and blue cycle represent the temporal topographic changes in summer and winter.

3.2 Hampyeong Bay

Figure 3-9 (a) and (b) represents the results of waterline extraction in Hampyeong Bay for the 1980s and the waterlines are shown in blue and red in the winter and summer, respectively. Background image is also NIR band of the Landsat 8 satellite, acquired on January 6 in 2014, when the tidal height was 114 cm. The tidal height ranges from 90 cm to 496 cm and from 69 cm to 481 cm in the winter and summer, respectively.

Figure 3-10 represents the generated DEMs of (a) winter and (b) summer during the 2010s using the extracted waterlines from 2010s Landsat images. The DEM was interpolated with a spatial resolution of 0.3 m and the boundary conditions, maximum and minimum height, were employed from the height ranges of each season. For the 2010s, the tidal height ranges from 45 cm to 489 cm and from 85 cm to 488 cm in the winter and summer, respectively.

Then, for quantitative estimate of the temporal topographic changes from 1980s to 2010s in the Hampyeong Bay, the maximum and minimum heights of both DEM_1980s and DEM_2010s winter and summer are modified to same height range from 90 cm to 481 cm, and from 85 cm to 488, respectively.

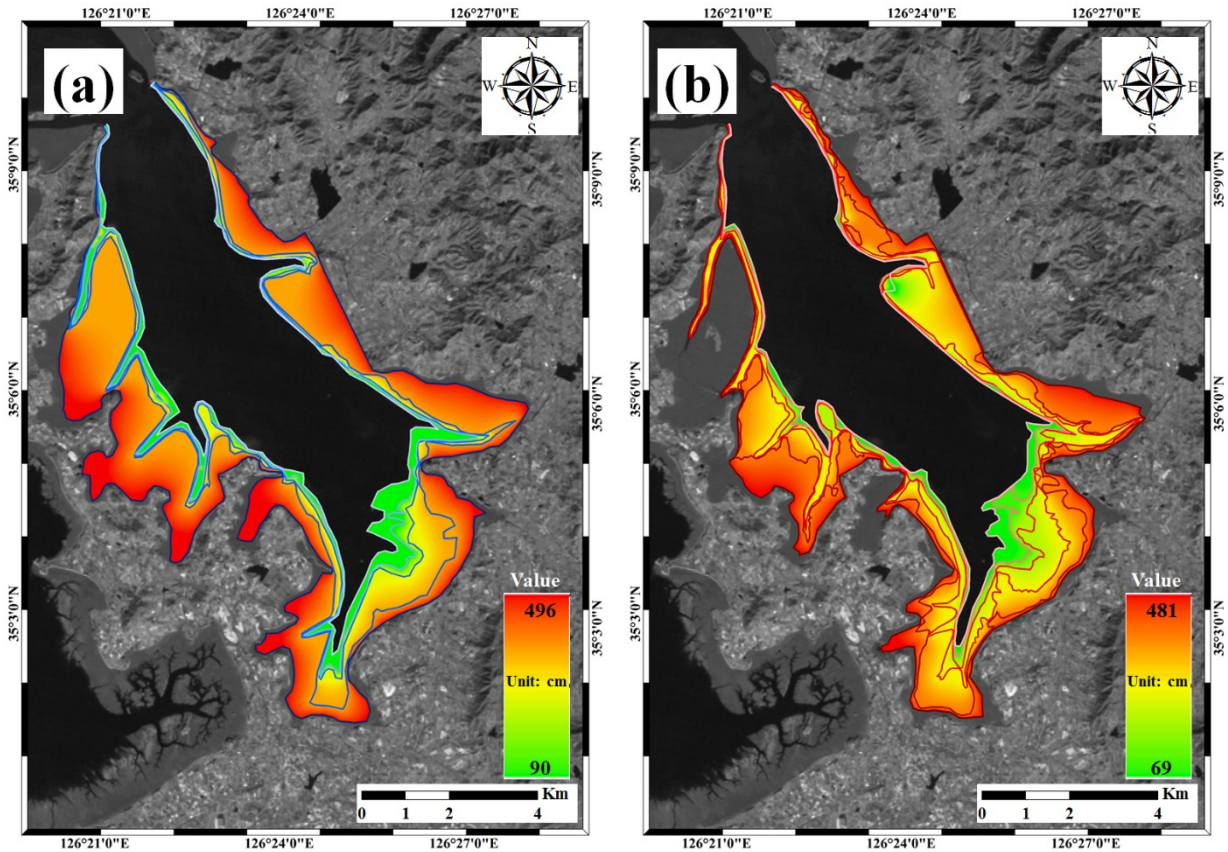

Figure 3-9. Waterline extraction and waterline generation in Hampyeong Bay on 1980s

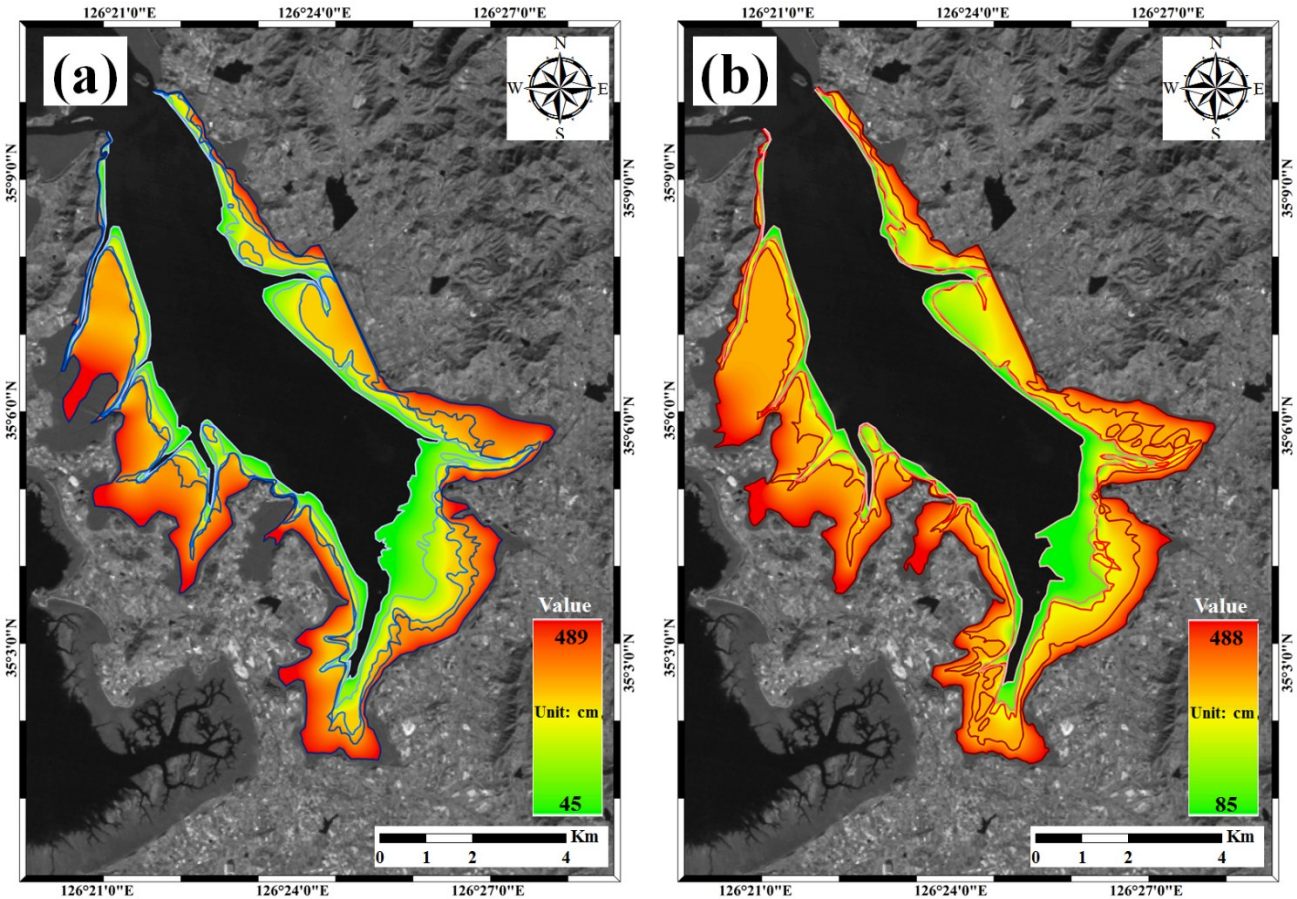

Figure 3-10. Waterline extraction and waterline generation in Hampyeong Bay on 2010s

Fig 3-11 show the spatially distribution of the topographic changes at the Hampyong Bay during 1980s to 2010s winter and summer seasons. The erosion effect was dominant in the Hampyeong Bay in both of winter and summer season. The deposition effect is more dominant in summer than the winter with about 11.6 cm in the Hampyeong Bay period of 1980s to 2010s (Table 3-4).

For the winter, erosion can be observed throughout the bay area. Deposition is observed in part of some areas in the interior of Hampyeong Bay. In summer also, erosion tends to be dominant in the entire Hampyeong Bay. However, the spatial distribution of deposition was slightly different when compared with the winter. That is, the deposition was mainly observed inside the bay in the winter; and yet, one can observe the deposition throughout the entire bay area in the summer.

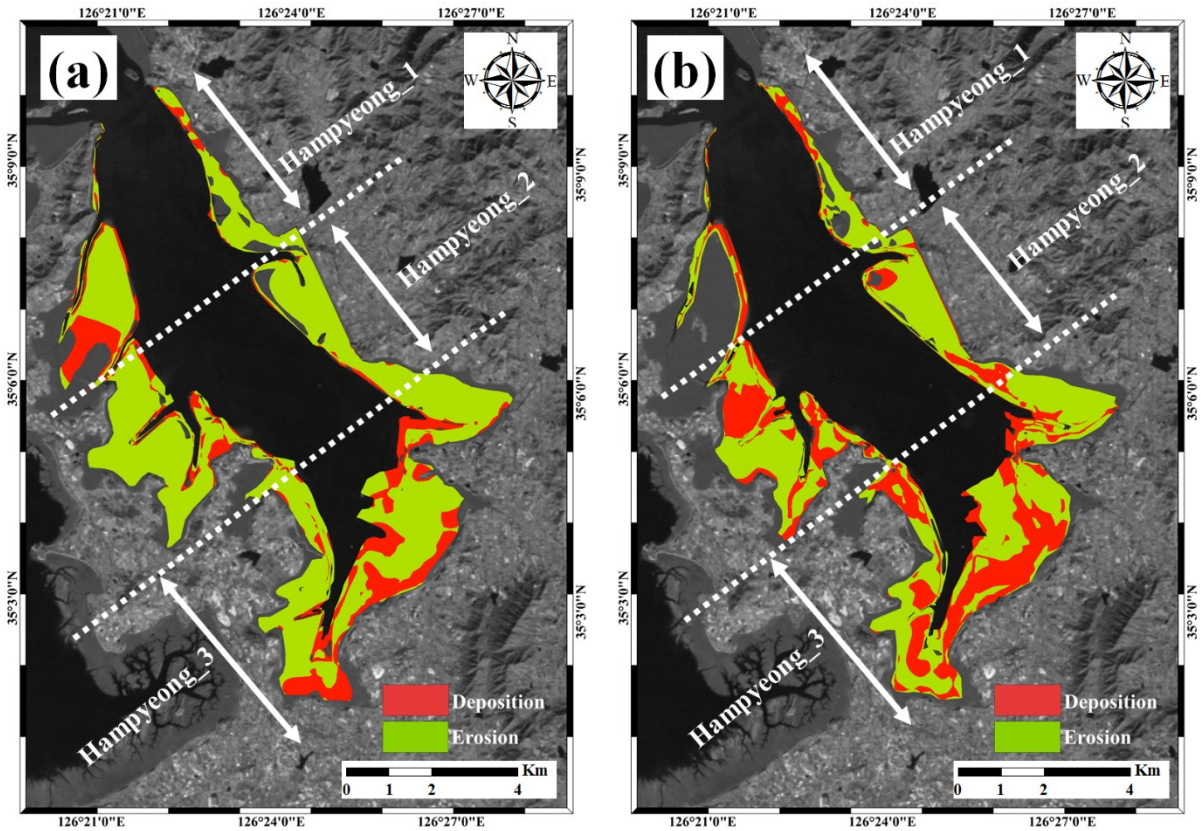

Figure 3-11. Spatial distributions of deposition and erosion are shown in red and green, respectively. The entire bays are split into 3 sections according to the length and formation shape of each bay. (a) winter; (b) summer.

Table 3-4. Hampyeong spatial distribution winter and summer

Bay	Season	Average topographic variation(cm)
Hampyeong_1	Winter	-38.3
Hampyeong_2		-46.0
Hampyeong_3		-19.5
Overall average topographic changes		- 34.6
Hampyeong_1	Summer	-47.5
Hampyeong_2		-15.7
Hampyeong_3		-75.5
Overall average topographic changes		-46.2

Similarly with Gomso Bay, the seasonal variation of intertidal topography was estimated quantitatively in the previous chapter. The result showed that the bay of Hampyeong showed a seasonal change of about -5 cm. Thus, this seasonal topographic variation was taken into consideration in the long term change between the 1980s and the 2010s. Figure 3-12 shows the final result of the long-term topographic since the 1980s; in the winter, erosion was about 29.6 cm and in the summer, erosion was about 41.2 cm.

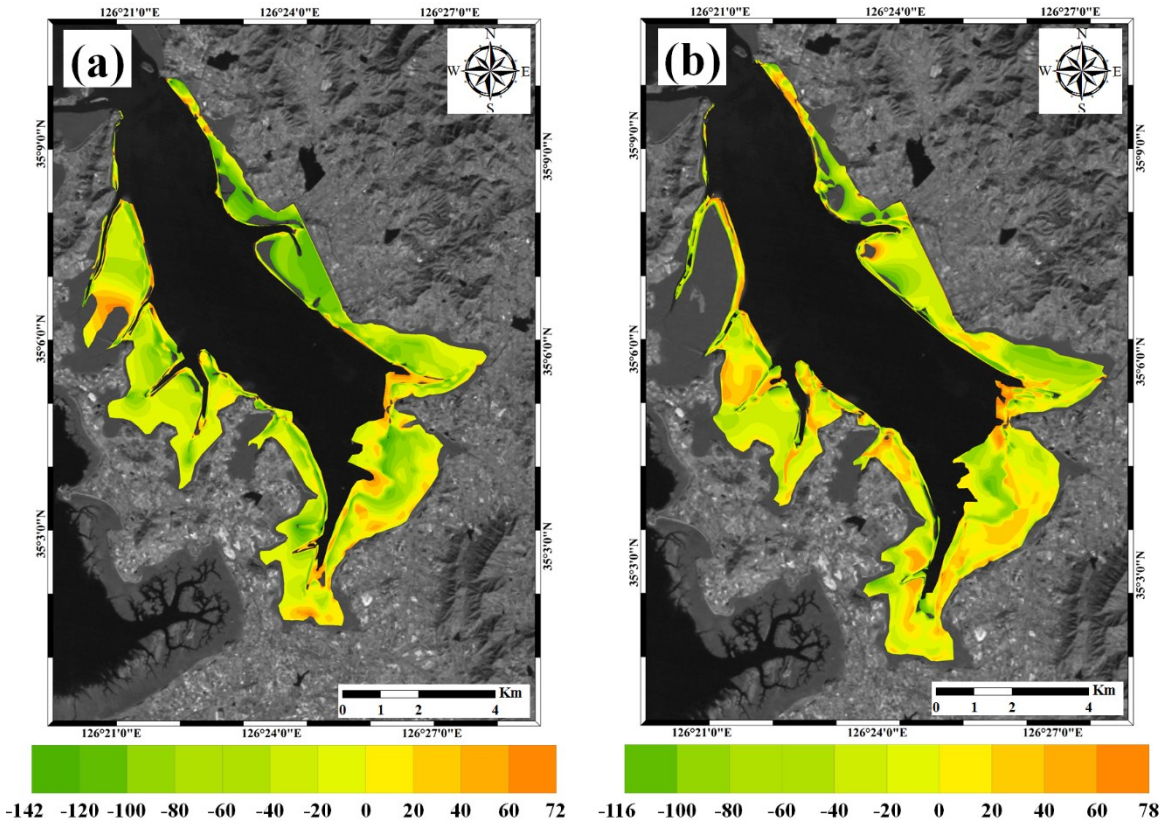

Figure 3-12. Estimation of topographic changes using waterline method during 1980s - 2010s. (a) Summer (b) Winter

The temporal topographic change analysis was performed, between 1980s to 2010s. The waterline extraction and DEM were generated using the 40 scenes of the Landsat 2, 3, 4, 5, 7, and 8 satellite images (Figure 3-13 and 3-14). We separate the outer (Hampyeong_1), middle (Hampyeong_2) and inner parts (Hampyeong_3) to analyze the temporal topographic changes in the Hampyeong Bay. A total of 19 scenes of Landsat images used to extract the waterlines and generate the winter season DEMs in each decade from 1980s to 2010s (Figure 3-13). A total of 21scenes of the Landsat images were used to extract the waterline and generate the DEMs in summer, from 1980s to 2010s (Figure 3-14).

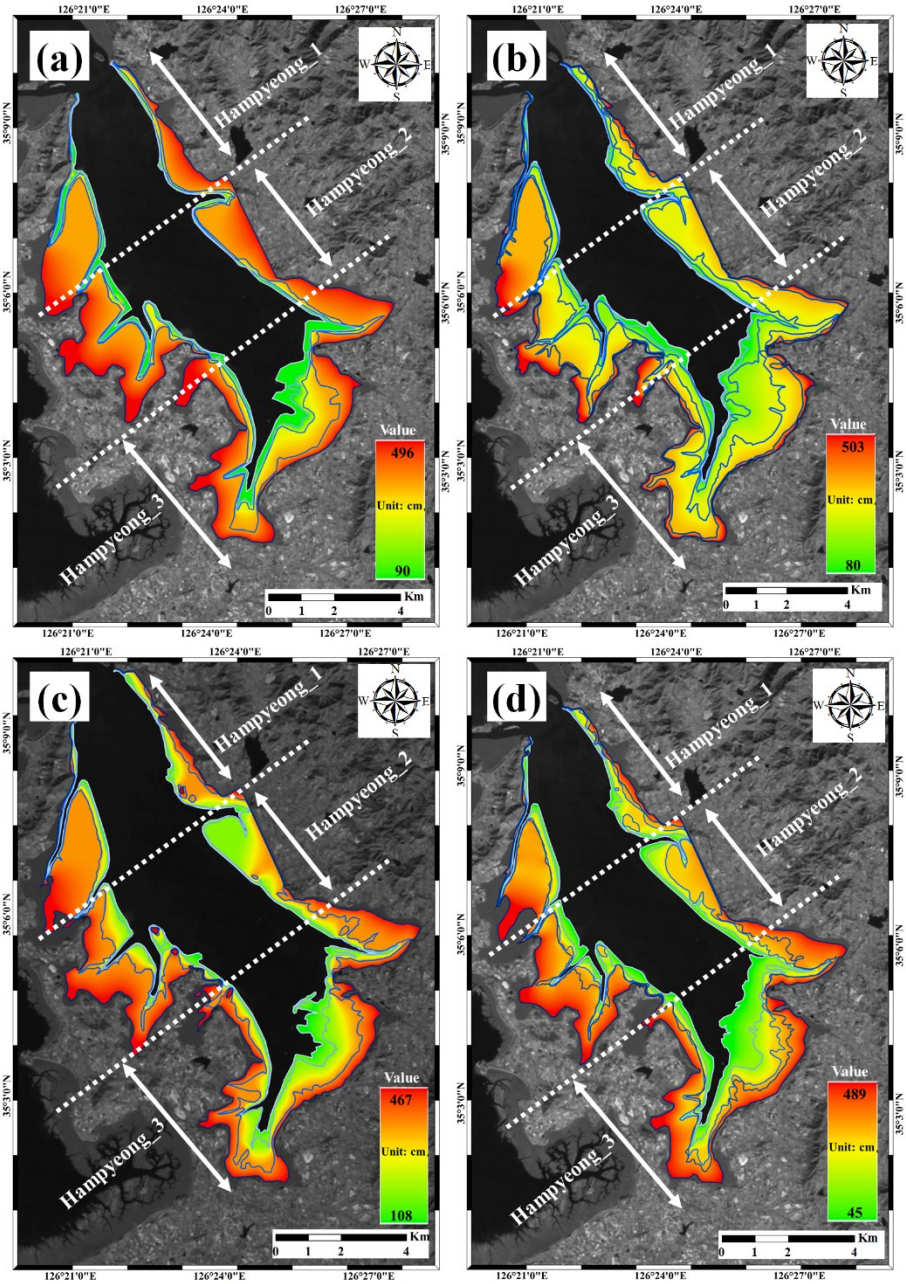

Figure 3-13. Results of waterline extraction and DEM generation using the winter season acquired Landsat images in each decade in the Hampyeong Bay, during the 1980s to 2010s. (a) 1980s; (b) 1990s; (c) 2000s; (d) 2010s

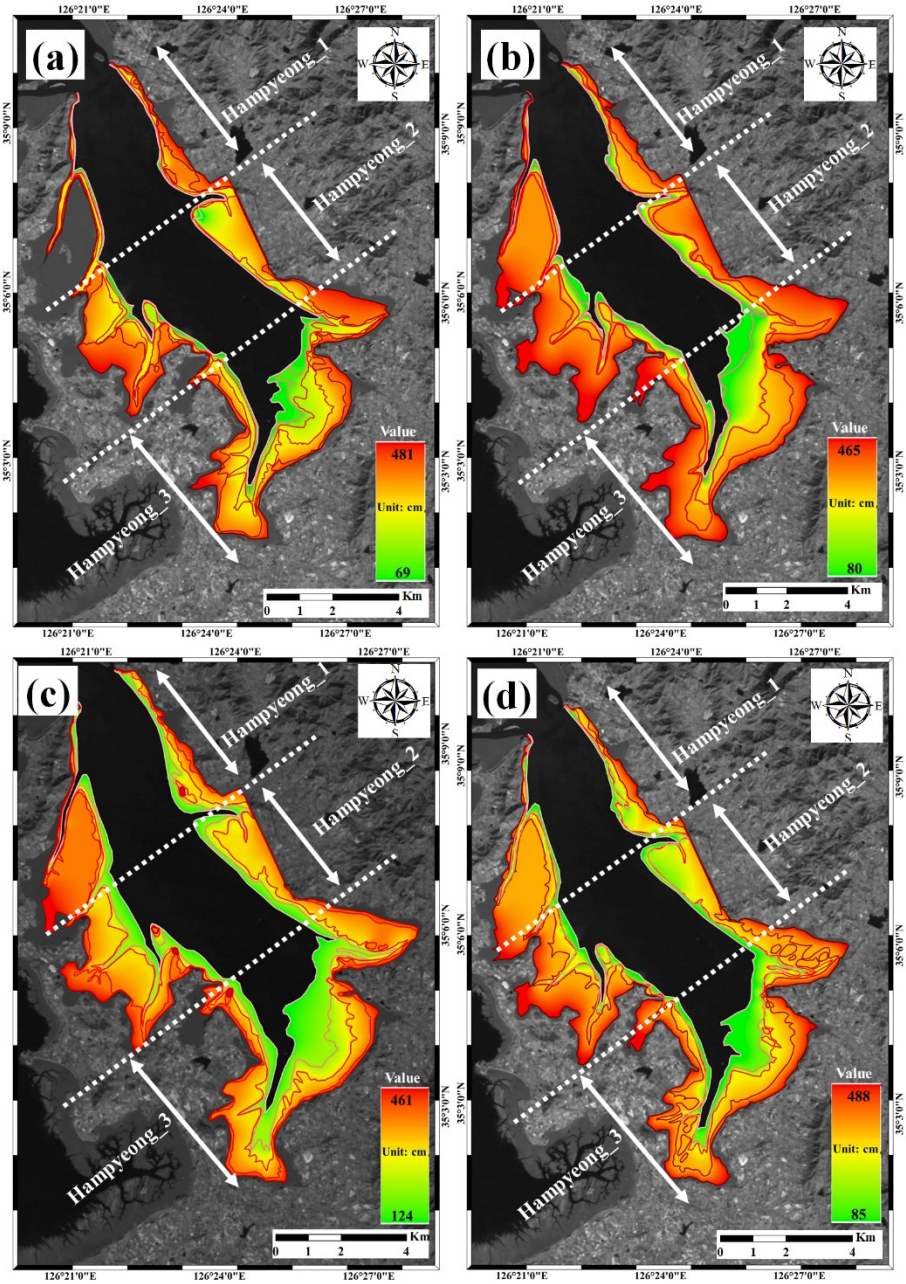

Figure 3-14. Results of waterline extraction and DEM generation using the summer season acquired Landsat images in each decade in the Hampyeong Bay, during the 1980s to 2010s. (a) 1980s; (b) 1990s; (c) 2000s; (d) 2010s

The results shows the temporal changes in each part of the Hampyeong Bay on both summer and winter season. In each part of the Hampyeong Bay, the erosion was dominant from the past to the present in the winter and summer (Figure 3-15).

Furthermore, the results show that, as the 2000s the topographic was not regularly deposited and eroded, it is similar to the Gomso Bay. It might be also effect on constructed big Saemangum sea dyke. However, in Hmapyeong bay, the distance between Saemanguem Sea dyke is more longer than Gomso Bay, therefore the less impact in the Hampyeong Bay.

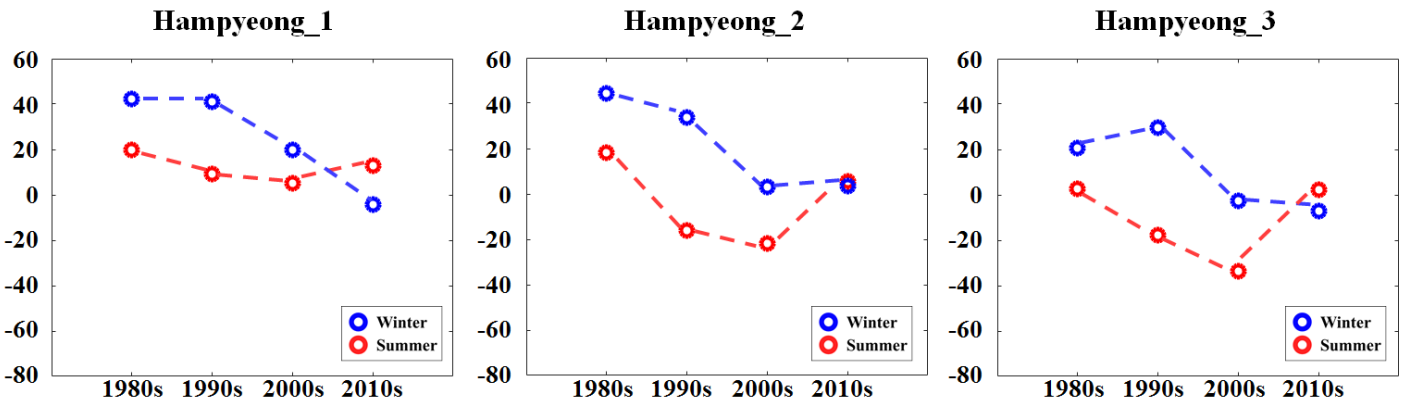

Figure 3-15. Temporal topographic changes in each part (outer, middle, and inner of the Hampyeong Bay) of the Hampyeong Bay, during 1980s to 2010s. The red cycle and blue cycle represent the temporal topographic changes in summer and winter.

4. Summary

In this chapter, the quantitative topographic change in Gomso and Hampyeong Bay was estimated based on the Landsat satellite image using the waterline method for period 1980s to 2010s. In Gomso Bay, deposition was predominantly observed in overall; whereas in Hampyeong Bay, erosion was dominant. In addition, deposition occurred more in the summer than the winter in Gomso Bay. In comparison, erosion appeared more clearly in the summer in Hampyeong Bay. These variation patterns spatially match with the seasonal topographic changes as the output from Chapter 2.

Finally, the topographic variation from the 1980s until the 2010s was calculated after the seasonal variation from Chapter 2 has been removed. As a result, Gomso Bay showed the predominant deposition regardless of the season. In the winter, the amount of deposition was about 12.4 cm; in the summer, the deposition was about 31.9 cm. For Hampyeong Bay, erosion was dominant in overall with the amount of 29.6 cm and 41.2 cm in the summer and winter, respectively.

Chapter 4. Estimation of Topographic Changes using SAR Interferometry

1. Introduction

Synthetic Aperture Radar (SAR) interferometry extracts three-dimensional topographic information of the surface using microwave phase difference of a single scattering target from two SAR data (Rogers and Ingals, 1969; Graham, 1974; Zebkeretal., 1994).

Research and application of SAR interferometry up to date has been limited in most inland areas. This was due to the influence of relatively smaller temporal decorrelation effect in inland areas than the coastal areas. SAR interferometry on coastal areas was first applied the New Orleans area of the United States and suggested the applicability of the method to interference in the coastal regions (Hong and Won, 2005). However, due to the influence of the unstable Doppler center frequency of ERS-2, PSInSAR has been proposed and been actively conducted (Arrigoni et al., 2003; Blanco et al., 2005; Wegmüller et al., 2005).

In the case of intertidal zone, it is difficult to maintain high interferometric coherence due to the ever-changing surface conditions. Therefore, the single-pass interferometry can be the most effective method for acquiring reliable interferogram to produce coastal DEM. TanDEM-X mission and SRTM are a couple of the single-pass SAR systems for which are highly suitable for generating a DEM of the intertidal zone.

In this study, the feasibility of SAR interferometry technique on monitoring the topographic variation of the intertidal zone is to be validated. The technique will be applied to the intertidal zone of Gomso Bay for a short-term and long-term topographic variation.

2. Material and Methodology

2.1 Data

In this chapter, the TanDEM-X and X-band SRTM data were used to estimate the temporal topographic changes in the Gomso Bay (Table 4-1).

The TanDEM-X mission (TerraSAR-X add-on for Digital Elevation Measurement) is based on two almost identical earth observation satellites: TerraSAR-X and TanDEM-X. Both are equipped with a modern, powerful radar system, a Synthetic Aperture Radar (SAR). It can be used to monitor the earth not only during the daytime but also at night and under cloud cover. In this chapter, two pairs of TanDEM- X data were used for generate the DEM with tidal height in 271 and 188 cm, respectively (Figure 4-1, Tabel 4-1).

Table 4-1. List of SAR data

Data	Acquisition date	Tidal height	Effective baseline
X-SAR SRTM	2000-02-17	123 cm	60 m
TanDEM-X	2012-11-27	271 cm	180 m
TanDEM-X	2015-06-12	188 cm	1271 m

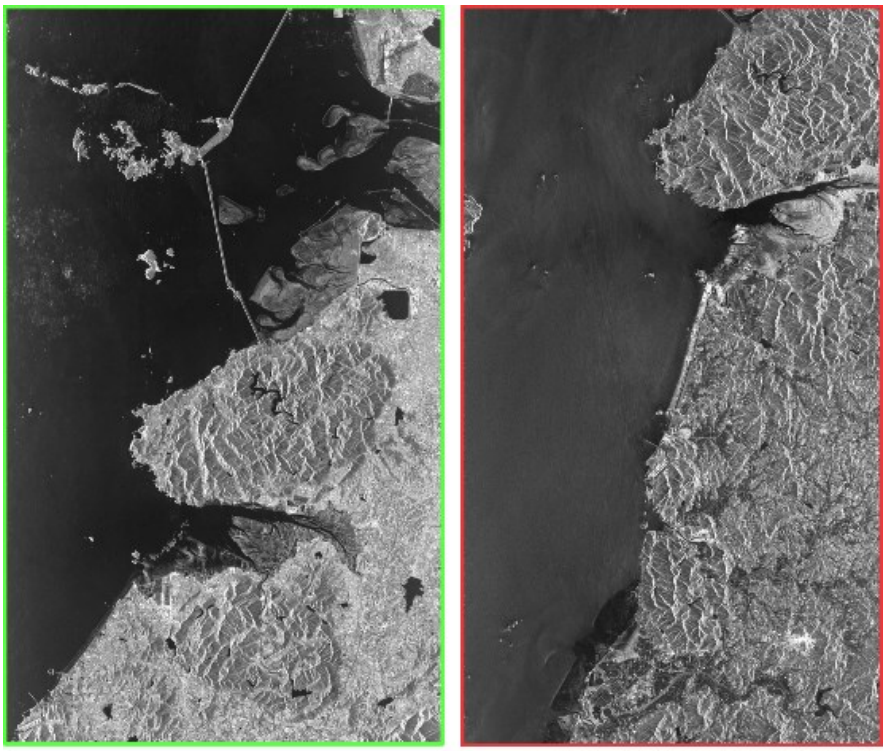

Figure 4-1. TanDEM data of used for generate DEM (Left: acquired on 2012. 11.27; right: acquired on 2015.06.12).

The Shuttle Radar Topography Mission (SRTM), flown on the Space Shuttle Endeavour on Flight STS-99 and launched on 11 February 2000, produced digital elevation data of the Earth's land mass between 60 degrees north latitude and 54 degrees south latitude. SRTM is a cooperative project of the National Aeronautics and Space Administration (NASA) and the National Imagery and Mapping Agency (NIMA) in the U.S.A., and the Deutches Zentrum tiir kuft und Raumfahrt (DLR) in Germany. The Italian Space Agency cooperated with DLR by contributing flight hardware previously flown in 1994, and by participating in data processing. For X-

band SRTM, the payload flew over Gomso Bay on February 7th in 2000 when the tidal height was 123 cm.

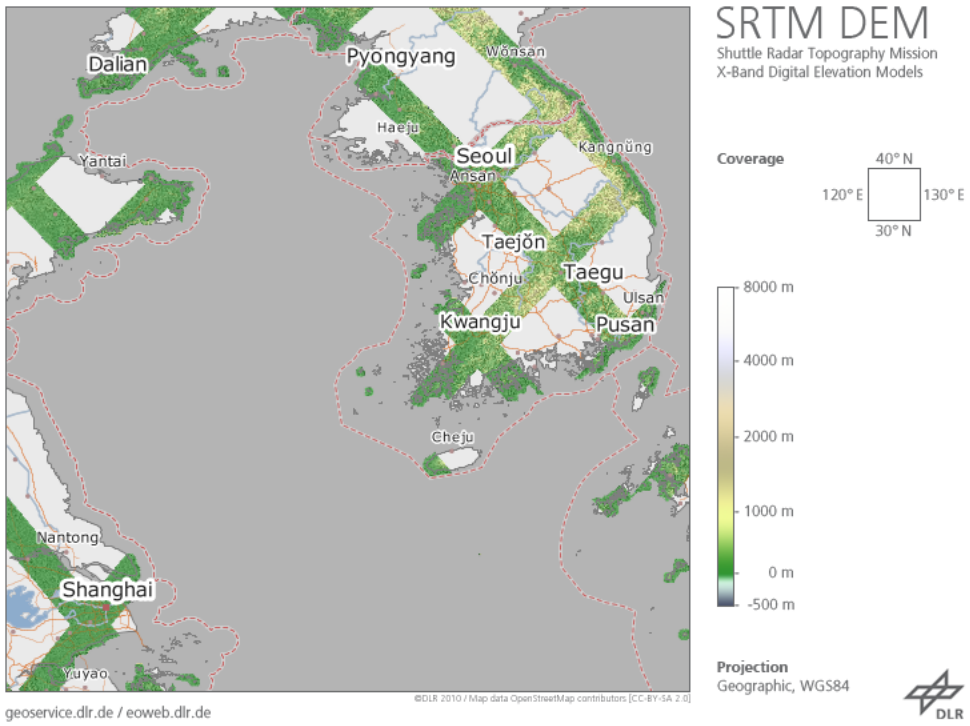

Figure 4-2. A part of SRTM observation track in South Korea (DLR).

2.2 Methodology

Conventional radar satellites transmit pulses of microwave energy and these are reflected from Earth's surface to be received again by the radar. The distance of the satellite from Earth's surface can be calculated from the round-trip transit time of the signals. As the satellite orbits Earth, the radar illuminates a strip of ground beneath it and records the reflected signals sequentially. After intensive signal processing a two-dimensional image of the area is generated. The received echo signals also contain information about the properties of the reflecting surface, such as its roughness.

SAR interferometry is a further development of this basic technique. The target land area is imaged from two different positions. The principle is similar to human stereoscopic vision, where depth perception – determining the distance of an object from the viewer – is achieved by viewing the object from slightly different angles with a pair of eyes. The 'radar eyes' are located on the satellites TerraSAR-X and TanDEM-X, which are orbiting Earth in close formation.

Because the satellites are a set distance or 'baseline' apart each other, the 'path length' that the signal travels as it is reflected back from each point on the ground will differ slightly for each of them and by measuring these differences precisely enough, elevation information can be derived. This is done by using the wave properties of the radar pulse and examining the relative time shifting of the waves due to the differing path lengths. This is also called 'phase difference measurement'. The result of performing these measurements for each point over an area of Earth's surface is

an interference pattern called an interferogram. From the measured differences in path length, the desired height information is obtained, with interference 'fringes' that resemble contour lines on a conventional map.

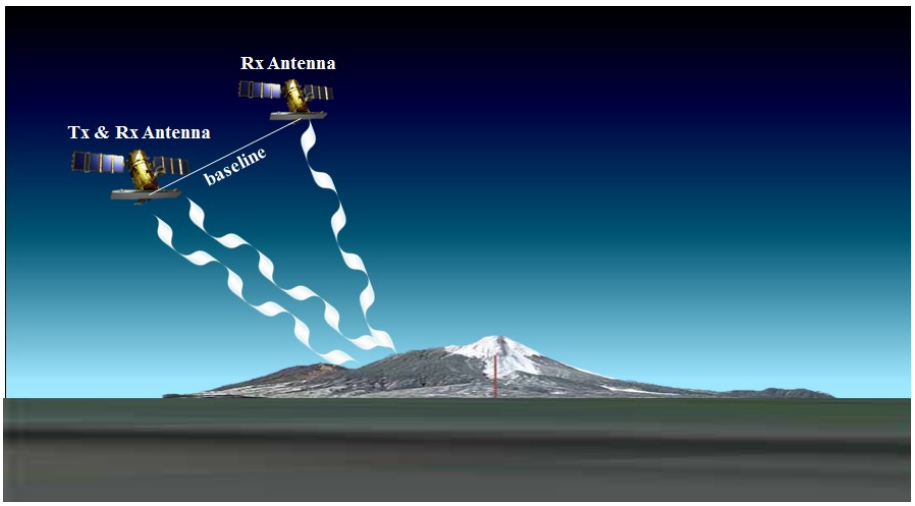

Figure 4-3. Illustration of satellite formation for SAR interferometry.

In this chapter, the typical interferometric processing technique was applied to generate a DEM using TanDEM-X data in the Gomso Bay. The interferometric processing chain is illustrated in Figure 4-4. This processing starts with spectral filtering to common spectra and high resolution image co-registration. Resampling of the slave image onto the master image is also conducted. Based on interferogram, we can obtain the flattened image. Baseline phase unwrapping including the calculation of cost-functions controlling the underlying minimum cost flow algorithm follows the flattened interferogram generation. An important step for accurate calibration of the DEM data is the determination of the (Ground Control Point) GCP. We use the National Standard Points which are provided from National Geographic Information Institute (NGII) to calculate the absolute height. The actual geocoding is based on the SRTM DEM together with a set of maps assessing the quality of estimated terrain height.

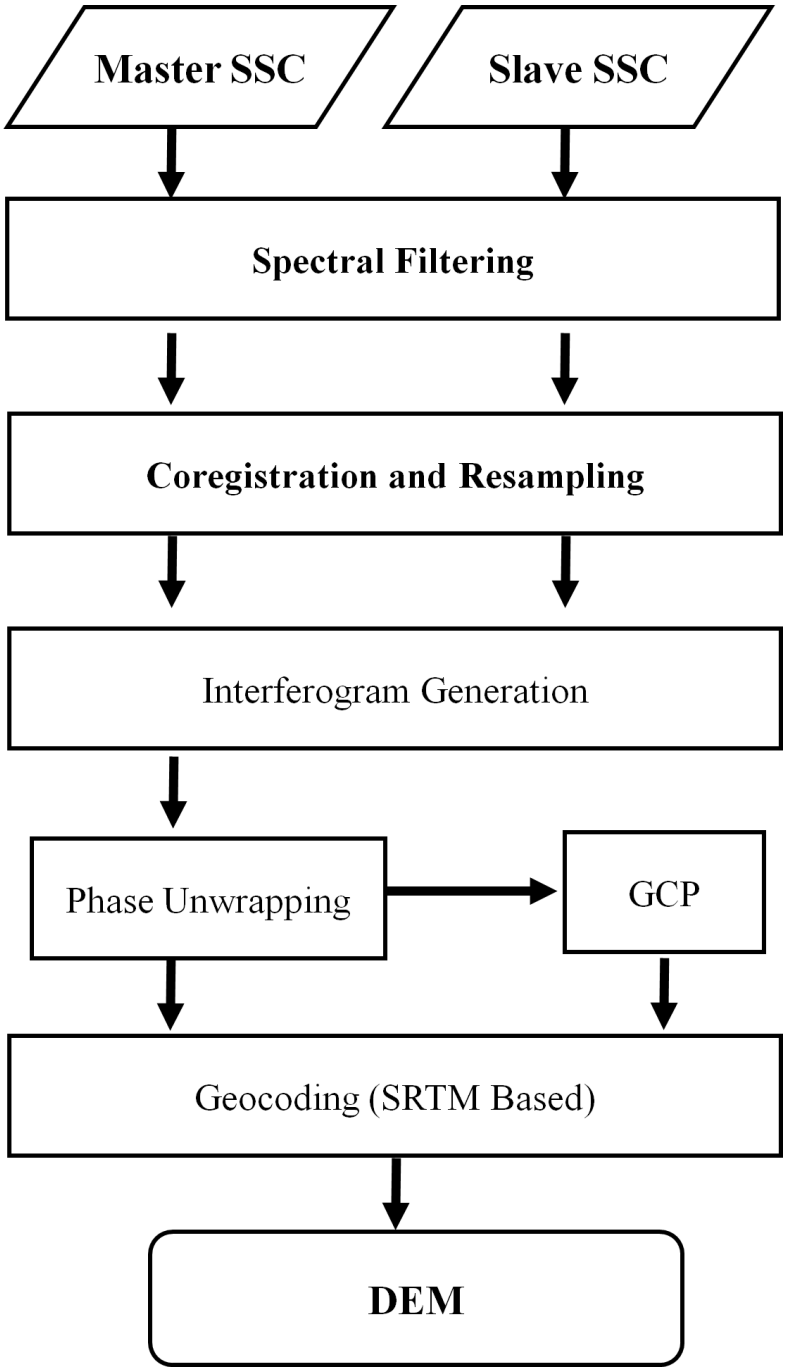

Figure 4-4. Generation of DEM processing.

2.3 Short- and Long- term topographic changes using SAR interferometry

In this chapter, the short (during 3 yrears)- and long-term (during 15 yrears)-topographic changes were estimated using the SAR interferometry technique in Gomso Bay, which is located at west coast of the Korean Peninsula. The 2012 and 2015 DEM were generated from the TanDEM data based on the SAR interferometry and the used TanDEM data were listed as Table 4-1. To estimate the topographic change, the 2012 DEM was subtracted from the 2015 DEM. Similarly, the long-term topographic change was estimated by subtracting the 2000 year DEM from 2015 DEM; for which the 2000 year DEM is extracted from the X-Band SRTM product. The estimation of short- and long-term topographic changes processing chain is illustrated in Figure 4-5.

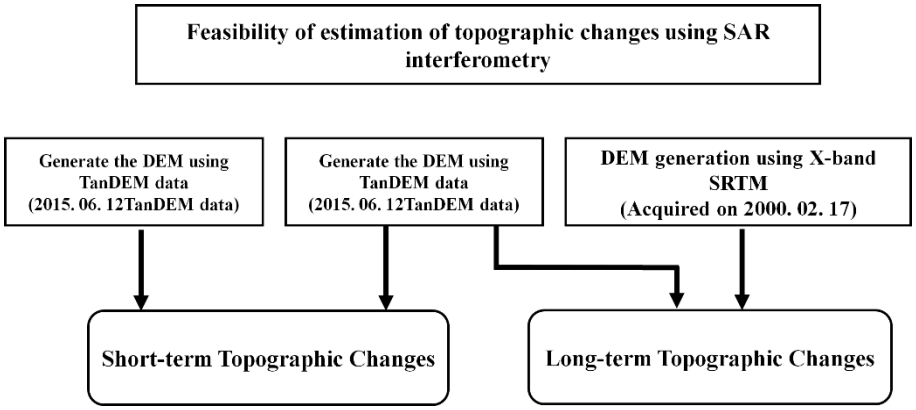

Figure 4-5. Flowchart of feasibility of estimation of topographic changes.

3. Study area

The study area is Gomso Bay, located in the southwestern coast of Korean peninsula. Gomso Bay is classified into the semi-closed coast tidal flat with a funnel-shaped embayment 7–9 km wide and 20 km long (Figure 4-6). The main tidal channel, with water depths up to 20 m, runs west-east in the northern part of the bay and its branch links to the Jujin Stream in the southern part of the shoreline. Mean tidal in this area has a range of 4.34 m and spring and neap tide are 5.90m and 2.78m, respectively. The maximum tidal current velocities in the main tidal channel are 1.2 ms-1 during a flood and 1.5 ms-1 during an ebb (Chang and Choi, 1998).

Furthermore, the Hampyeong Bay was also included in the study area for GPS measurement site (Figure 4-6b). More detailed geology and environmental information were described at the Chapter 2.

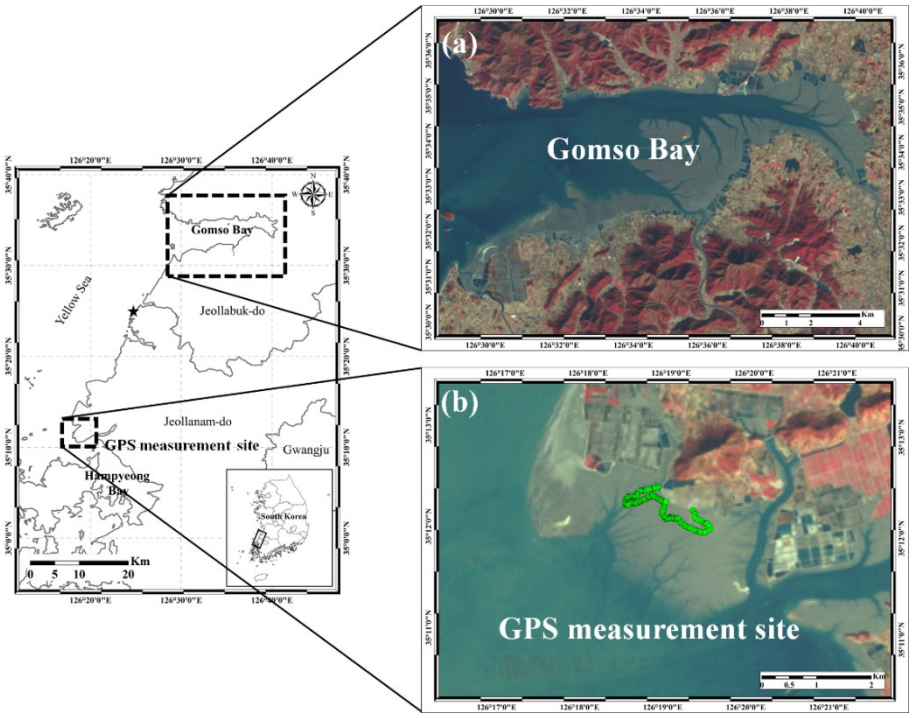

Figure 4-6. Study area of Chapter 4, located at west coast of South Korea.

4. Accuracy assessment

The accuracy assessment of the generated DEMs was performed which from TanDEM-X data. Two pairs of the TanDEM data were used to generate the DEM for accuracy assessment. The RTK-GPS measurements was performed near the mouth of the Hampyeong Bay (Figure 4-7b), the detailed specification of Leica Viva GNSS GS15 see Appendix.

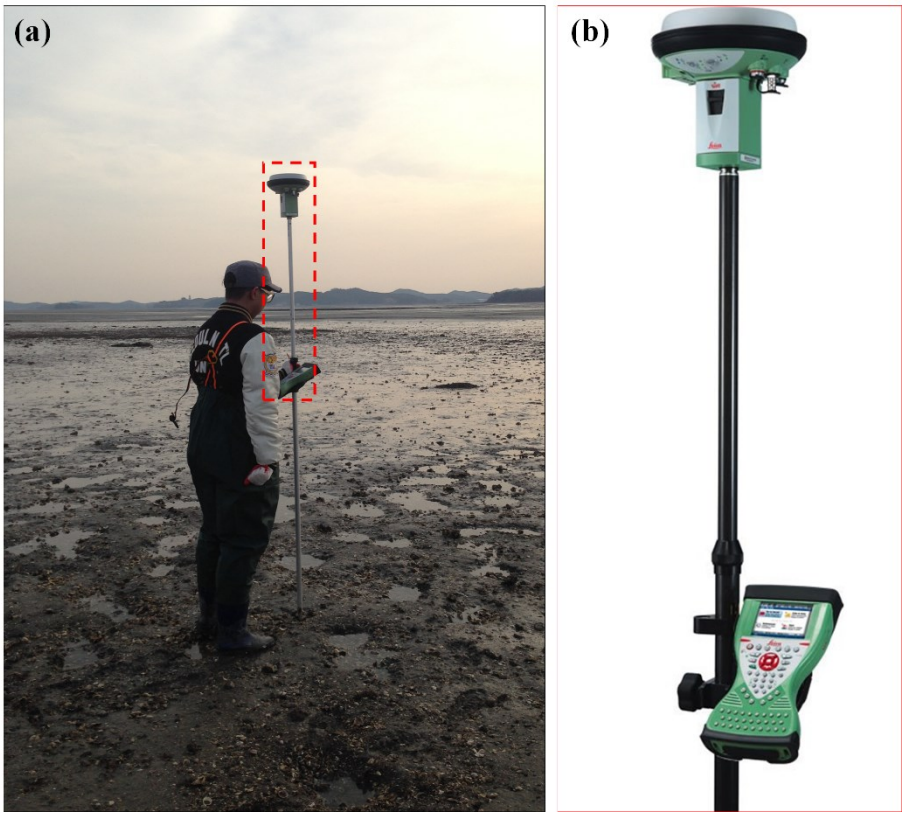

Figure 4-7. GPS measurement (a) using the Leica Viva GNSS GS15 (b).

For accuracy assessment of the generated DEM from TanDEM data, the two pairs of TanDEM data was acquired in the Hampyeong Bay, which has similar baseline and date to the Gomso Bay TanDEM data (Figure 4-8; Table 4-2)

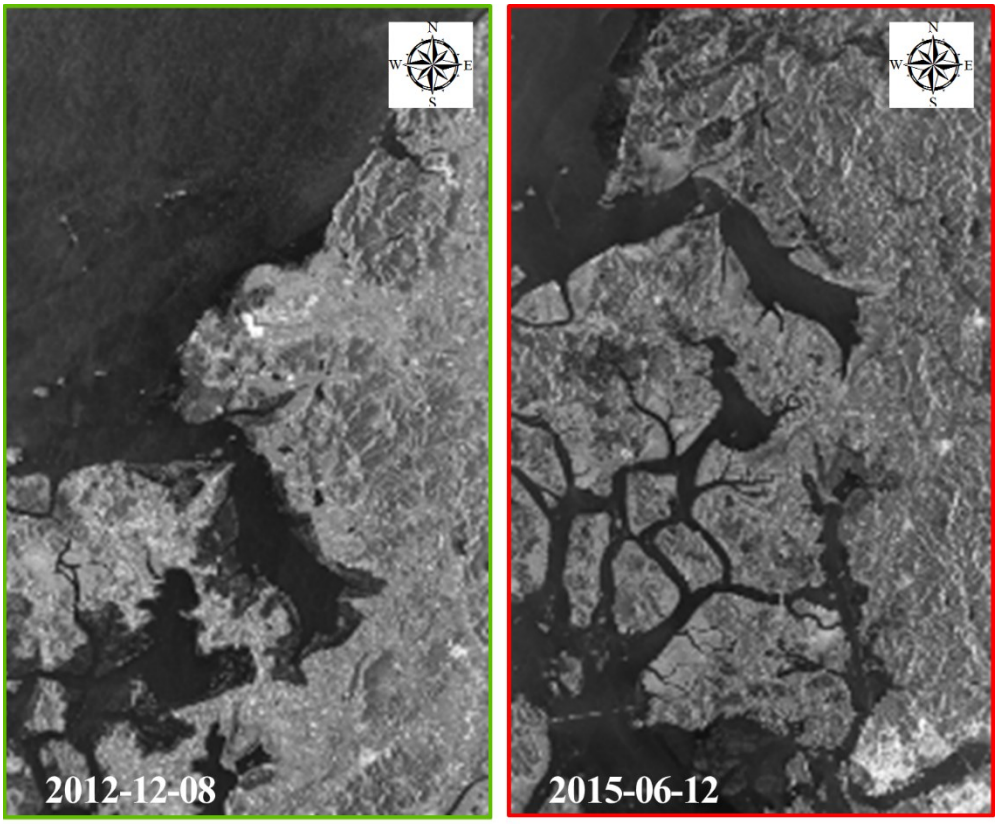

Figure 4-8. TanDEM data for accuracy assessment of generated DEM, acquired at 2012-12-08 and 2015-06-12.

Table 4-2. Information of the TanDEM data for accuracy assessment in Hampyeong bay test site.

Data	Acquisition date	Tidal height	Effective baseline
TanDEM-X	2012-12-08	251 cm	171 m
TanDEM-X	2015-06-12	166 cm	1280 m

The GPS data was acquired on 28th December, 2015 and 14th January, 2015 near the outer of the Hampyeong Bay. A total of 209 points of the GPS data was acquired by RTK-GPS measurements in Hampyong bay (Table 4-3).

Table 4-3. GPS measurement in the GPS measurements site near the mouth of Hampyeong Bay.

Date	Number of points
2015.12.28	89
2016.01.14	120
Total	**209**

5. Results and discussion

Figure 4-9 and 4-10 show the results of the profile comparison. The results of error analysis are summarized in Table 4-4. DEM extracted from TanDEM data acquired at 8th December 2012 has the higher errors than the other DEMs which were extracted from images acquired in 2015. Because of relatively high ambiguity height, the 8th June DEM is sensitive to phase error of interferogram. If the instrument only has a few degrees of error, it could be converted to 1 m scale height difference with real value. Thus, the long effective baseline DEMs are suitable for providing topography of tidal flat including microstructure like channels.

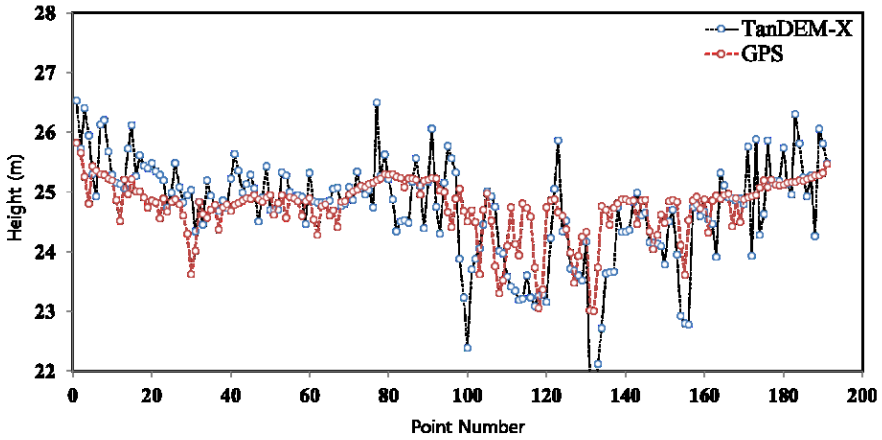

Figure 4-9. Height comparison of between DEM and GPS measurement data (8th August, 2012).

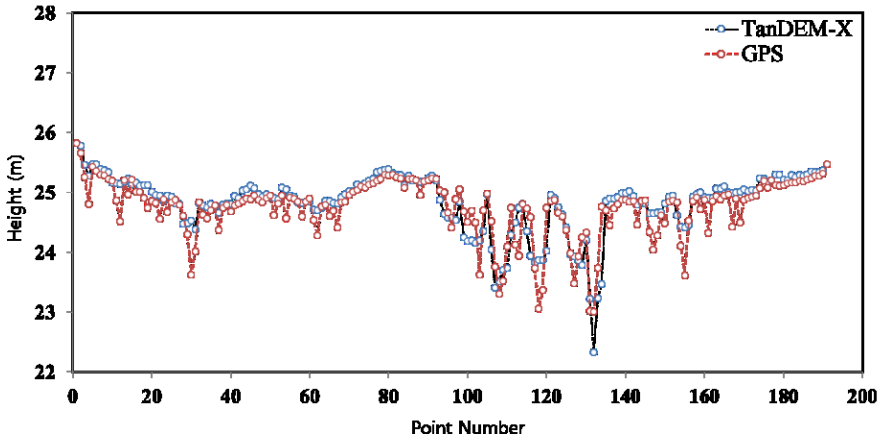

Figure 4-10. Height comparison of GPS measurement data and generated DEM which from TanDEM data acquired on 12th June , 2015.

Table 4-4. Accuracy assessment of generated DEM from TanDEM data in Hampyeong Bay.

Acquisition Date	Effective Baseline	Ambiguity Height	Mean Coherence	Mean SNR	Incidence angle	RMSE
2012-12-08	171 m	60 m	0.86	12.3	34.7	**0.72 m**
2015-06-12	1280 m	3.6 m	0.64	26	28.8	**0.25 m**

Coherence of the interferogram is an important criterion for the feasibility. The main task will be to find elements controlling coherence in tidal flats. Tidal conditions must be one major element influencing to coherence. However, there are additional elements including surface water cover, surface roughness, sand ripples, etc. The 1-2 cm deep surface water remains for a considerable time even after the bottom surface is fully exposed, which seriously affect backscattering. This problem is more serious in mixed or mud flats than in sand flats. Surface roughness, especially r.m.s. height, is a critical parameter to backscattering, and consequently the change in surface roughness would result in incoherent interferometric phases.

The coherence map was created using the 2 pairs of TanDEM-X data over the Gomso Bay, which were used data were acquired on the 27th November, 2012 and 12th June, 2015 (Figure 4-11). The Figure 4-11(a) was represent the coherence map of relative short-baseline (180 m) TanDEM-X data in this study, which used remote sensing data was acquired on the 27th of November, 2012. The Figure 4-11(b) shows the coherence map relative long baseline (1271 m) TanDEM-X data, which used data was acquired on the 12th of June, 2015. The coherence was high maintaining about 0.9 in the short-baseline TanDEM data, and with 0.65 in the case of long-baseline TanDEM-X data. From the results, the coherence is higher in the short-baseline than in the long-baseline, in the Gomso Bay. It was a general phenomenon, because of the coherence have high relation to the length of baseline.

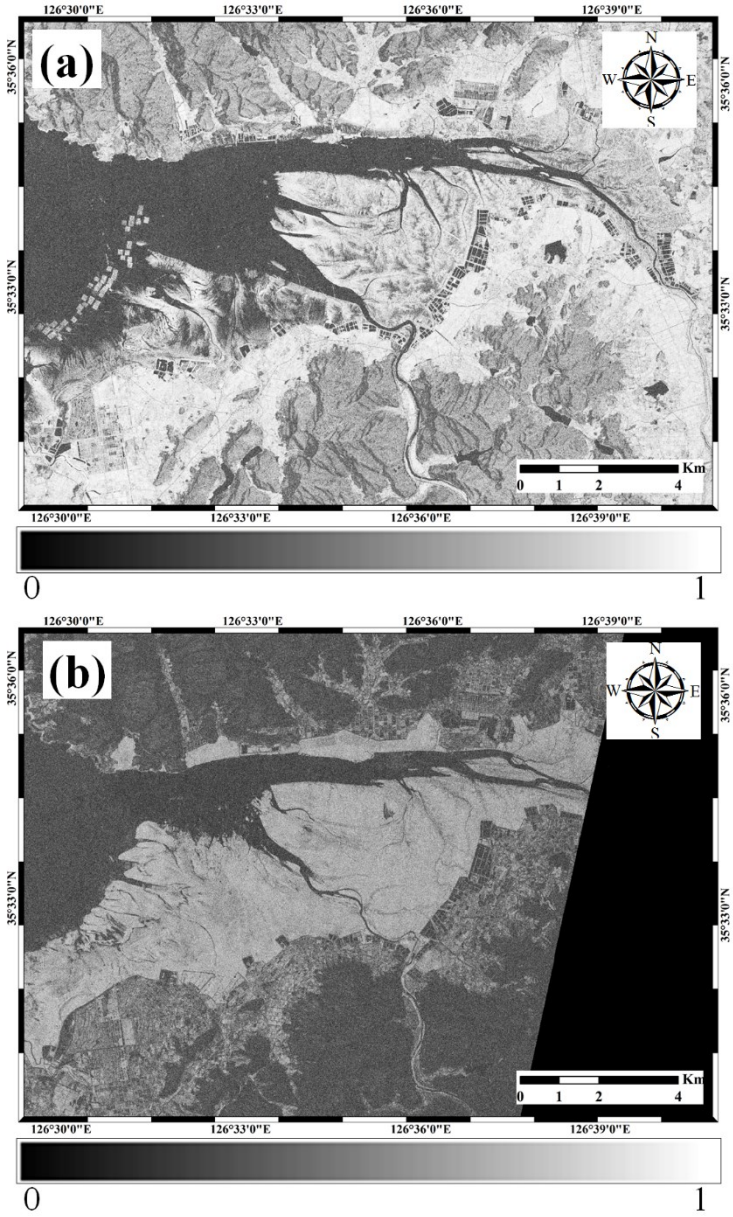

Figure 4-11. Coherence map of TanDEM-X pair in the Gomso Bay, in 27th November (a), 2012 and 12th June, 2015 (b).

Also the interferogram were generated in the Figure 4-12, from the relative short and long baseline TanDEM-X data, in this study.

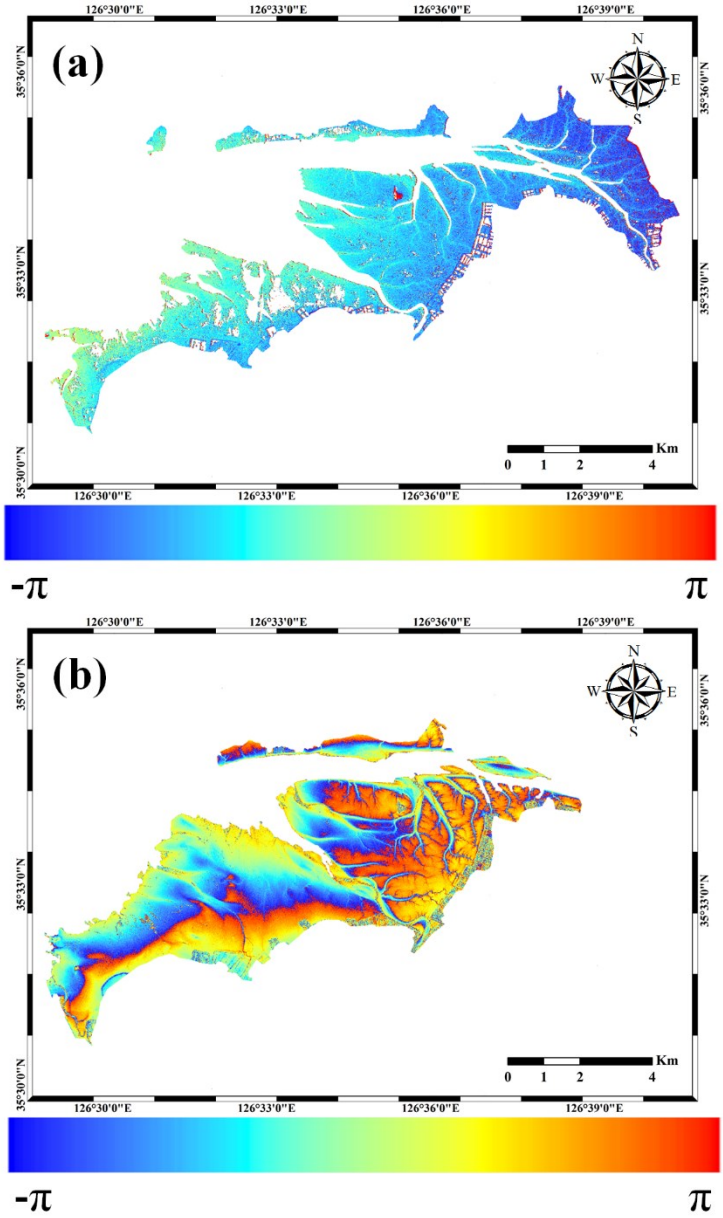

Figure 4-12. The interferogram of an TanDEM-X pair in Gomso Bay, the used data were acquired on 27th November (a), 2012 and 12th June, 2015 (b).

From the 2 pairs of TanDEM-X data, we succeeded in unwrapping the interferometric phase and constructing a DEM in Gomso Bay. Figure 4-13 represents the short-term topographic changes based on the SAR interferometry using TanDEM data, which were acquired on 27th November, 2012 and 12th June, 2015. Figure 4-13(a) shows the generated TanDEM DEM in 2015, and the generated height range was from -5cm to 736 cm. Figure 4-13b shows the generated TanDEM DEM in 2012 with the height ranges from -6 cm to 736 cm. In order to estimate the short-term topographic changes in the tidal flats in Gomso Bay, the 2012 DEM was subtracted from the 2015 DEM; and the result is shown in Figure 4-13c. The overall change was deposition of 3 cm during 3 years.

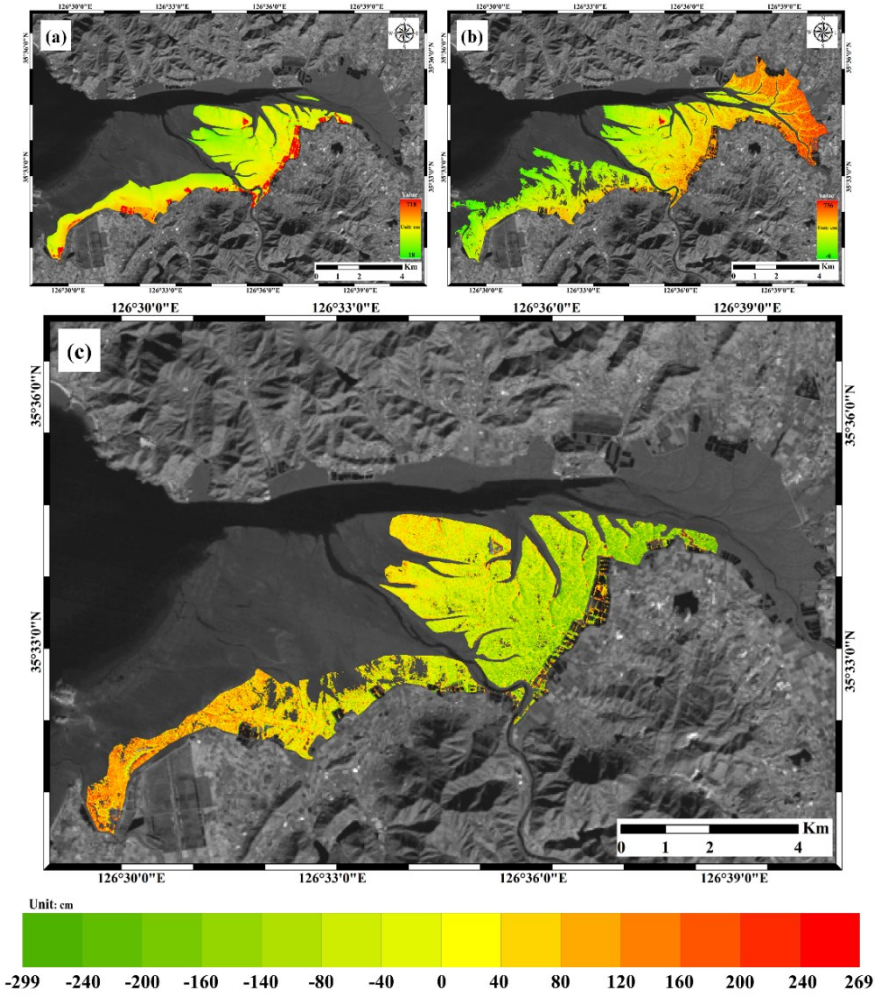

Figure 4-13. Result of Generated DEM based on the SAR interferometry using TanDEM data, (a) 27th November, 2012; (b) 12th June, 2015. Quantitative results of topographic changes during 2012 to 2015 (c).

Figure 4-14 represents the topographic changes based on the waterline method between 2003 and 2004 using Landsat images. More detailed methodology and information about used data was described in Chapter 2. The comparison of the topographic changes, derived from SAR interferometry and the waterline method, was performed. Because of the difference of the time span between the results, the spatial trend of deposition and erosion was analyzed. In both results, the deposition was observed around the main tidal channel, and the erosion was distributed near the coast. In overall, the deposition was predominant in both cases.

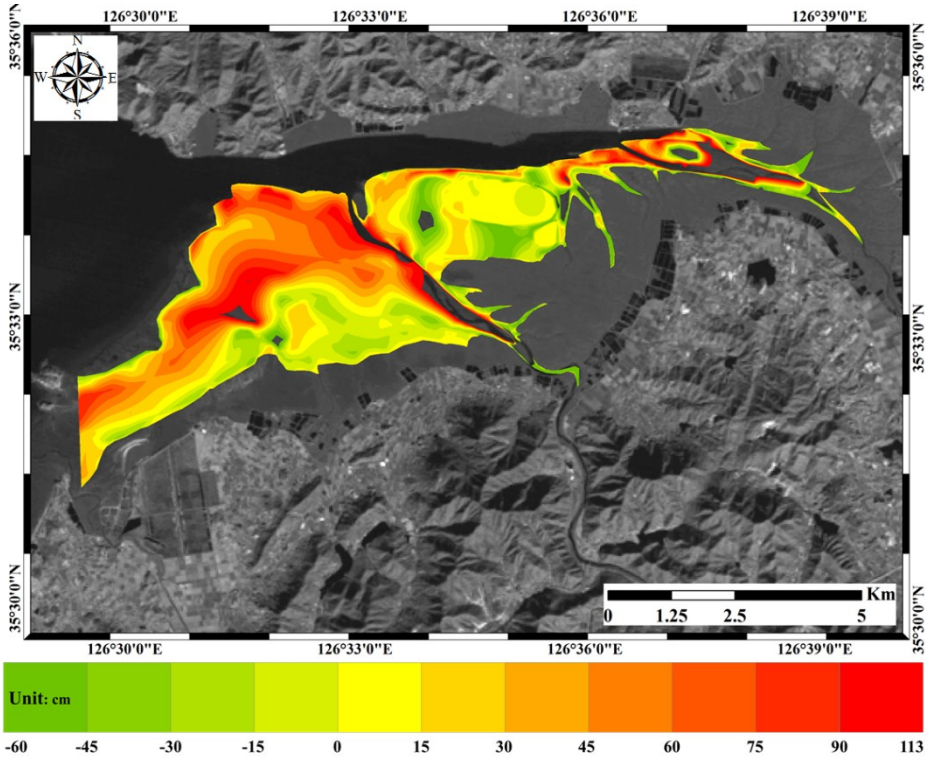

Figure 4-14. Result of topographic changes using waterline method during 2003 to 2004

Figure 4-15(a) and 4-15(b) shows the generated DEM from TanDEM data and the product of X-band SRTM data. Figure 4-15(c) represents the topographic changes between TanDEM-X and X-SAR SRTM data (i.e. Tan2015_DEM minus X-SAR_DEM) from 2000 to 2015 in Gomso Bay. The overall average topographic change was -229 cm.

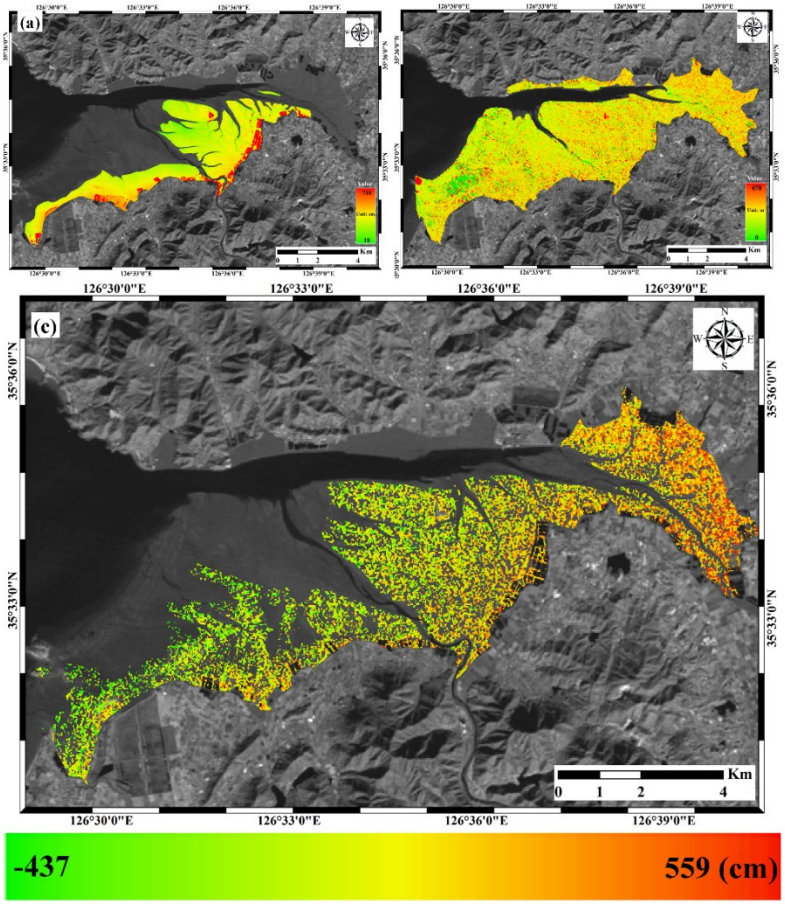

Figure 4-15 Generated DEM using SAR interferometry technique using TanDEM data(a); X-SAR SRTM data(b). Result of topographic changes using the SAR interferometry technique during 2000 to 2015(c).

Figure 4-16 (a) and (b) represents the results of waterline extraction in the Gomso Bay by the digitizing through visual investigation method, during 2003 and 2013 year, respectively. The background image corresponds to the NIR band of the Landsat 8 satellite image, acquired on 6th January, 2014, when the tidal height was 116 cm. Each line represents tidal heights ranging from 25 cm to 456 cm, and 46 cm to 469 cm during 2003 to 2013, respectively.

Figure 4-16 (a) and (b) also represents the generated DEM during 2003 (2003_DEM) to 2013 (2013_DEM) using the extracted waterlines. The DEMs were interpolated with a spatial resolution of 0.3 m and the boundary conditions, maximum and minimum height, were employed from the height ranges of 2003_DEM and 2013_DEM. Then, the maximum and minimum heights of both 2003_DEM and 2013_DEM were bounded to 456 and 46 cm, respectively, to rule out the amount difference caused by the extent mismatch in the study area.

The temporal topographic changes, i.e., 2013_DEM minus 2003_DEM, are shown in Figure 4-16 (c). Green color (red color) depicts that height of the tidal flat is higher (lower) in past than in present. The positive and negative values represent the deposition and erosion over the study area during 2003 to 2013. The deposition effect is dominant in the Gomso Bay, with approximately 11.5 cm topographic changes.

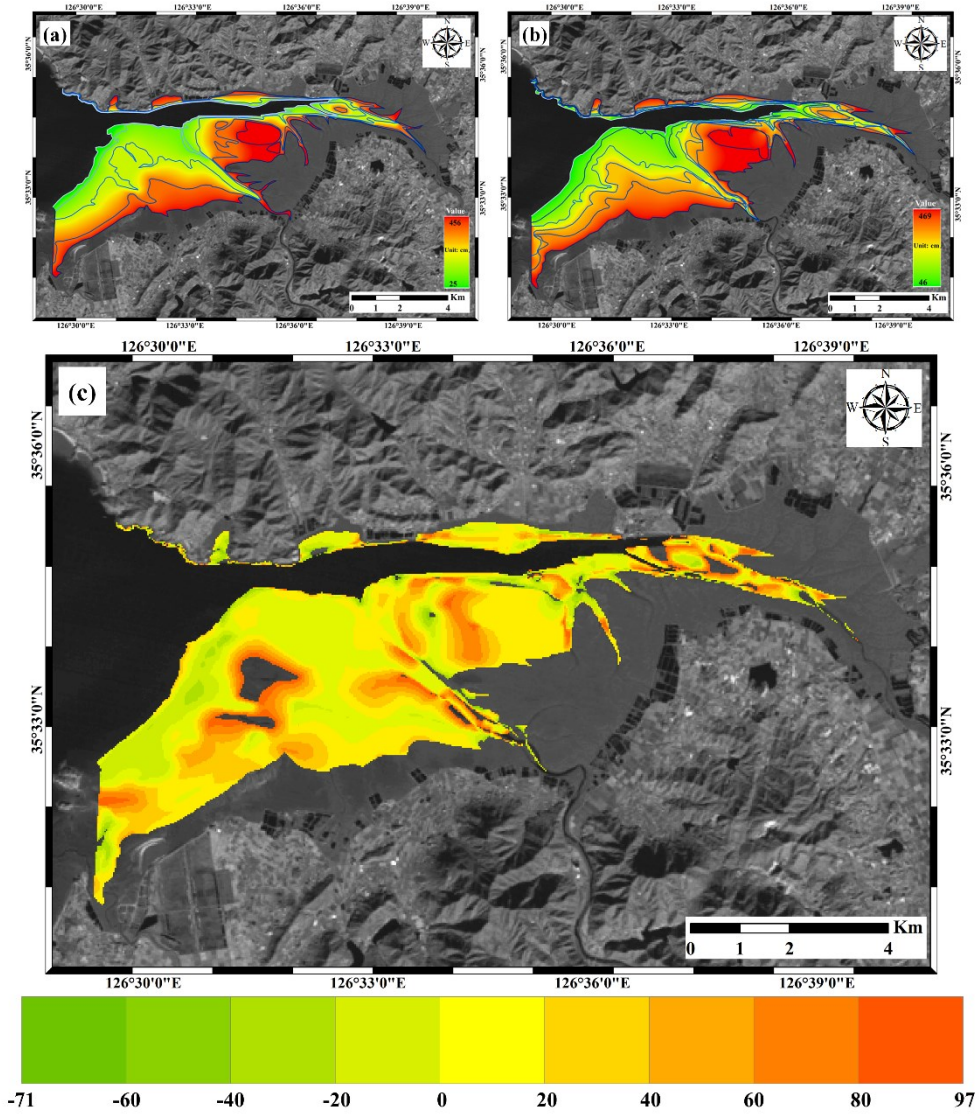

Figure 4-16. Results of waterline extraction and generated DEM in Gomso bay, (a) 2003 year; (b) 2013 year. Quantitative results of topographic changes during 2003 to 2013 (c).

The comparison of long-term topographic changes results was performed which using SAR interferometry technique and waterline method. There is no similar trend of topographic change between the results from SAR interferometry and waterline method. In addition, the overall average topographic changes using the SAR interferometry was -229 cm, it is preposterous value to compare to the overall average topographic changes using waterline method.

The reason as follow:

The altitude of ambiguity has high correlation with the accuracy of the DEM height. The altitude of ambiguity ha is defined as the altitude difference that generates an interferometric phase change of 2π after interferogram flattening. The altitude of ambiguity is inversely proportional to the perpendicular baseline:

$$h_a = \frac{\lambda R \sin\theta}{B_n} \qquad (2)$$

Where, λ is wave length, R is perpendicular baseline, θ is incidence angle, and B_n is perpendicular baseline.

Table 4-5. Parameter of X-SAR SRTM and TanDEM.

	Incidence angle (θ)	**Wavelength (λ)**	**Altitude of satellite height (R)**	**Perpendicular Baseline (Bn)**
X-SAR	33.0 degree	9.6 Ghz	233,100 m	60 m
TanDEM	33.8 degree	9.65 Ghz	514,000 m	1271 m

The altitude of ambiguity height was calculated, using the Equation 2. The altitude of ambiguity is about 2 m in the case of X-band SRTM data, and in case of TanDEM data was used in this chapter, the altitude of ambiguity height was about 79 m. Therefore, X-band SRTM product is not represent the topography of Gomso Bay.

6. Summary

In this study, the short-term and long-term topographic changes of tidal flats in Gomso Bay were estimated based on SAR interferometry technique utilizing TanDEM X-band SRTM data were attempted.

As a result, the short-term changes of tidal flats, derived from TanDEM-X data between 2012 and 2015, are calculated and showing a similar trend with the changing terrain observations of the same area using the waterline method. On the other hand, the long-term result for 15 years by comparing X-band SRTM and TanDEM-X has shown that the result is not reliable. Because of high ambiguity height due to a short baseline of X-SAR SRTM; unable to show relatively flat surface of tidal flats effectively. In addition, areas with low interferometric coherence of X-band SRTM over tidal flats are excluded during the signal processing.

However, the possibility of monitoring topographic change of tidal flats using SAR interferometry technique is high enough. In the future, it is expected to provide more datasets to study the variation in time series when the single-pass SAR data are accumulated over tidal flats.

Chapter 5. Conclusion

The seasonal and temporal topographic variations of Gomso and Hampywong Bay tidal flats in south korea were estimated and evaluated using various remote sensing data and techniques, the topography of tidal flats in Gomso and Hampyeong Bay was constructed using the waterline method applied to acquired Landsat images. Then, the seasonal topographic variation of tidal flats was evaluated by subtracting the winter topography from the summer. The result showed that summer deposition is the dominant effect in Gomso tidal flats with an average overall seasonal topographic change of 12.8 cm. In contrast, summer erosion is dominant with -5.0 cm topographic variation in Hampyeong Bay. From the results we observed that Gomso and Hampyeong Bay are though classified as semi-enclosed coast tidal flat, the sedimentary facies caused by formation geometry and sediment type led to different topographic changes.

The estimated topographic change during the 1980s to 2010s, with combining the results of the seasonal topographic change the minimum topographic changes were derived in the western coast of Korea peninsular for about 30 years. The results show that, the topographic variation between 1980s and 2010s was calculated after the removal of seasonal variation from Chapter 2. As a result, Gomso Bay showed the predominant deposition regardless of the season. In the winter, the amount of deposition was about 12.4 cm; in the summer, the deposition was about 31.9 cm. For Hampyeong Bay, erosion was dominant in overall with the amount of 29.6 cm and

41.2 cm in the summer and winter, respectively.

Finally, the feasibility of SAR interferometry technique for monitoring topographic variation in tidal flats has been evaluated. The topography of tidal flats in Gomso Bay derived from TanDEm-X bi-static interferometry and SRTM mission data are compared with those from the waterline method. Although the temporal difference between the datasets prevented from direct topographic comparison, the spatial trends of deposition and erosion were similar to those from the waterline method. However, there exists some limitations of long-term topographic monitoring using X-SAR SRTM and TanDEM-X interferometry because of large height of ambiguity caused by short baseline, 60 m in this study. Still, the potential of monitoring topographic variation of tidal flats using SAR interferometry is significant if more single-pass interferometry SAR data, such as TanDEM-X, are collected in time series.

In this study, SAR interferometry and the waterline method were studied to evaluate topographic changes of tidal flats. These are some of the various methodological limitations while performing this research.

For the waterline method, it is recommended to acquire image data in a short period of time with a different water level in order to obtain a good quality of the DEM. However, because of the nature of satellite trajectory assigned to the specified time, the time span of the obtained data corresponding to the various tide became inevitably long. Furthermore, the quality of the data is extremely sensitive to the effect of weather. These factors increase the time span of the data to several months, and sometimes even to many years. Therefore, the effort to collect the data in a short time span to reflect the representative topography changes was necessary.

In addition, the waterline method is required for tidal information which is necessary to assign to the waterline extracted from satellite images. Therefore, if the tide gauge is not installed in the area, it becomes extremely difficult to estimate the correct altitude for the waterline. Also, the precision of generated DEM becomes low.

Finally, the waterline is given a lot of influence on the extremely climate, such as typhoons and storms. Thus, even at the same tide level, the position of waterline is pronounced in accordance with the occurrence of storms and hurricanes. Such waterlines acquired after these extreme weather conditions causes a large error in the generation of DEM.

Such SAR interferometry technique applied in tidal flats are prone to experience greater difficulty than the land. In the case of the intertidal zone, maintaining high interferometric coherence is the biggest problem due to constantly changing surface conditions from tide to tide. Thus, single-pass interferometry might be the sole solution for utilizing interferometry for generating DEMs of tidal flats. In reality, TanDEM-X is the only space-borne SAR system which enables a single-pass interferometry. Moreover, a lack of past data limits temporal analysis. These results and challenges undoubtedly will provide a scope for future research.

Appendix

Table. Basic technical specifications of satellite positioning system LEICA VIVA GS15.

System Differential GPS Corrections	
1.0	The GPS system consisting of two receivers interchangeable between each other with supporting accessories, software to perform all the required applications.
Receiver GPS GNSS	
2.0	Have receivers of four (4) frequencies for both GPS and GLONASS satellites on. Also be able to receive signals from the third frequency GPS L5 and GALILEO satellites and the new L2C frequency for better and faster fix.
2.1	2.1 Each receiver offers 120 channels and two frequencies L1 and L2 on simultaneous detection of up to 60 satellites at both frequencies. The receiver performs measurements of phase and frequency waves two carriers L1 and L2 code measurements and C / A and P in L1 and L2 frequencies. Each receiver has: • Sixteen (16) channels of continuous detection of the frequency of L1. • Sixteen (16) channels of continuous detection of the frequency of L2. • Sixteen (16) channels of continuous detection of the frequency of L1 GLONASS and sixteen (16) channels of continuous detection of the frequency of L2 GLONASS + (4) SBAS (WAAS, EGNOS, GAGAN, MSAS)
2.2	Ability to record observations in kinematic and static procedure for post-editing in the office.

2.3	The rate of measurements' recording to qualify by 0.05 sec to 300 sec. The angle of the satellite measurements for recordings (cut - off angle) to be eligible.
2.4	The refresh rate of the position to be eligible by 0.05sec (20 Hz) to 1 sec (1Hz).
2.5	The system offers complete reference design parameters (availability of satellites, static figures Precision PDOP, GDOP, and azimuth angles of the satellites, sky map) all the data is tabular and graphical format.
2.6	Has built-in anti-jam mining on both frequencies L1 and L2.
2.7	Have reliable technology of reception under trees.
2.8	The mobile receiver to receive network RTK corrections and supports networked RTCM messages type of issue until v3.1.
2.9	The receiver is controlled via the serial port to any other program that runs on any platform.
2.10	The data from both receivers are recorded in CF Compact Flash or SD cards in both the receiver and the keyboard with selectable by the user to register.
2.11	The ISDN cards have at least 1GB of memory
2.12	The mobile receiver (rover) communicates with Bluetooth built-in antenna for kinematic and REAL TIME applications.
2.13	The rover receiver (mobile) consists of the antenna, keyboard, batteries and pole 197 with the support and its weight is not more than 3.5Kg.
2.14	The operating temperature range of the receiver is-30° C.-65° C.
2.15	The storage temperature range of the receiver is -40° C.
2.16	The resistance to humidity is 100% (total precipitation).
2.19	The RTK is fully integrated in receivers.

2.20	The integrated software of the receiver allows and the following measurements: • Surveying • Identification of reference systems • Mapping of all methods of orientation (north, sun, point, line, arrow navigation) • COGO applications for determining coordinate points with many geometric methods. Specifically: cuts straight to the field in straight distance calculations, arrows, shift, speed tracks, routes • Transformation etc. The user has the ability to create its own set of rules for all applications supported by the system and planning at the office before the field measurements.
2.21	The software has the ability to create lines and polygons as well as the possibility of introducing coding points, lines and polygons.
RTK performance	
3	The reliability of positioning should be better by 99.99%
3.1	For Real Time approach to achieving the following accuracies: Position 10mm +1 ppm; Elevation 20mm +1 ppm.
3.2	Continuously independent continuous control algorithms to resolve the ambiguity phase.
3.3	Equipment modem and GSM modem are removable from the receivers

	and not integrated.
3.4	To be making points with a frequency of 20Hz (0.05sec) without degradation of accuracy.
3.5	Time for On-the fly positioning in Real Time situation is 8 sec (typical) after connecting to satellites.
3.6	The display controller to display continuously the situation to resolve ambiguities.
3.7	The display controller to provide all information as the number of detectable satellites and the condition of the battery or memory card capacity.
3.8	The display controller to display graphic signs with engraving.
3.9	The system to read signs marking just ASCII files.
3.10	The scheme to import and export files onboard ASCII measurement sites offline with a program on a PC in a format of choice.
3.11	The system can import and export onboard DXF files points / lines / polygons without connection to program in a computer.
3.12	The system must support connection to GSM. The connection between the GPS receiver and GSM modem to be without power.
3.13	The system has the possibility of simultaneous wireless modem, and GSM modem in the body of the receiver.

References

Ahn, C., Lee, Y., Yoo, H., Oh, J., 1989. Application of satellite data on geomorphological study of the tidal flats near Keum river estuary. Journal of Korean Society of Remote Sensing 5, 2-15.

Ahn, K., Lee, H., Kim, D., 2011. DEM Generation of Tidal Flat in Suncheon Bay Using Digital Aerial Images. Korean Journal of Remote Sensing 27, 411-420.

Alexander, C., Nittrouer, C., Demaster, D., Park, Y., Park, S., 1991. Macrotidal mudflats of the southwestern Korean coast: a model for interpretation of intertidal deposits. Journal of Sedimentary Research 61.

Allen, J., 2000. Morphodynamics of Holocene salt marshes: a review sketch from the Atlantic and Southern North Sea coasts of Europe. Quaternary Science Reviews 19, 1155-1231.

Allen, J., and Pye, K., 1992. Coastal saltmarshes: their nature and importance. Salt Marshes, Morphodynamics, Conservation and Engineering Significance. Cambridge University Press, Cambridge, 1-18.

Arrigoni, M., Colesanti, C., Ferretti, A., Perissin, D., Prati, C., Rocca, F., 2003. Identification of the location phase screen of ERS-ENVISAT permanent scatterers, Proceedings of FRINGE 2003 Workshop, Frascati, Italy.

Anderson, F., Black, L., Watling, L., Mook, W., Mayer, L., 1981. A temporal and spatial study of mudflat erosion and deposition. Journal of Sedimentary Research 51.

Anderson, F., and Mayer, L., 1984. Seasonal and spatial variability of particulate matter of a muddy intertidal flood front. Sedimentology 31, 383-394.

Blanco, P., Mallorqui, J., Navarrete, D., Duque, S., Prats, P., Romero, R., Dominguez, J., arrasco, D., 2005. Application of the coherent pixels technique to the generation of deformation maps with ERS and ENVISAT data. Proceedings of IGARSS 2005, 1983-1986.

Chang, J., Kim, Y., Cho, Y., 1999. Tidal-flat sedimentation in a semienclosed bay with erosional shorelines: Hampyong Bay, west coast of Korea. The Sea 4, 117-126.

Chang, J., and Choi, J., 2001. Tidal-flat sequence controlled by Holocene sea-level rise in Gomso Bay, west coast of Korea. Estuarine, Coastal and Shelf Science 52, 391-399.

Chang, J., and Choi, J., 1998. Seasonal Accumulation pattern and preservation potential of tidal-flat sediments: Gomso Bay, west coast of Korea. Journal of the Korean Society of Oceanography 3, 149-157.

Chen, L., and Rau, J., 1998. Detection of shoreline changes for tideland areas using multi-temporal satellite images. International journal of remote sensing 19, 3383-3397.

Choi, J., Eom, J., Ryu, J., 2011. Spatial relationships between surface sedimentary facies distribution and topography using remotely sensed data: example from the Ganghwa tidal flat, Korea. Marine Geology 280, 205-211.

Chun, S., Lee, H., Ryu, S., Yang, B., 1998. Seasonal and local variation of sedimentation on the wave-dominated tidal flats, southwestern coast of Korea: comparison between inner-bay and open tidal flats. Proceedings of 15th International Sedimentological Congress.

Chun, S., Yang, B., Lee, I., Lee, H., 2000. Non-barred open macrotidal flat strongly influenced by wave action, Gomso Bay and Baeksu Coast, southwest Korea: depositional processes, seasonal evolution and transgressive stratigraphy: Tidalite-2000, 5th International Conference on Tidal Environments, Field Guide Book (B2).

Cracknell, A., 1999. Remote sensing techniques in estuaries and coastal zones an update. International Journal of Remote Sensing 20, 485-496.

De Jonge, V., Van Beusekom, J., 1995. Wind-and tide-induced resuspension of sediment and microphytobenthos from tidal flats in the Ems estuary. Limnology and oceanography 40, 766-778.

Deronde, B., Houthuys, R., Debruyn, W., Fransaer, D., Lancker, V. Henriet, J., 2006. Use of airborne hyperspectral data and laserscan data to study beach morphodynamics along the Belgian coast. Journal of Coastal Research, 1108-1117.

Eineder, M., Bamler, R., Adam, N., Breit, H., Suchandt, S., Steinbrecher U., 2000. SRTM/X-SAR Interferometric Processing-First Results. EUSAR 2000, 233-236.

Farr, T., and Kobrick, M., 2000. The Shuttle RadarTopography Mission: A Global DEM, IGARSS Proceedings 2000.

Frey, R., Howard, J., Han, S., Park, B., 1989. Sediments and sedimentary sequences on a modern macrotidal flat, Inchon, Korea. Journal of Sedimentary Research 59.

Frostick, L., and McCave, I., 1979. Seasonal shifts of sediment within an estuary mediated by algal growth. Estuarine and Coastal Marine Science 9, 569-576.

Gade, M., Alpers, W., Melsheimer, C., Tanck, G., 2008. Classification of sediments on exposed tidal flats in the German Bight using multi-frequency radar data. Remote sensing of environment 112, 1603-1613.

Graham, L., 1974. Synthetic Interferometer Radar for Topographic Mapping, Proceedings of IEEE 62,763-768.

Green, E., Mumby, P., Edwards, A., Clark, C., 1996. A review of remote sensing for the assessment and management of tropical coastal resources. Coastal management 24, 1-40.

Greidanus, H., Huising, E., Platschorre, Y., Van Bree, R., Van Halsema, D., Vaessen, E., 1999. Coastal DEMs with cross-track interferometry. Proceedings of IGARSS 1999, 2161-2163.

Heygster, G., Dannenberg, J., Notholt, J., 2010. Topographic mapping of the German tidal flats analyzing SAR images with the waterline method. IEEE Transactions on Geoscience and Remote Sensing 48, 1019-1030.

Hong S., and Won J., 2005. ERS-ENVISAT cross-interferometry for coastal DEM construction, Proceedings of FRINGE 2005 Workshop, Frascati, Italy.

Hoja, D., Lehner, S., Niedermeier, A., Romaneessen, E., 2000. DEM generation from ERS SAR shorelines compared to airborne crosstrack InSAR DEMs in the German Bight. Proceedings of IGARSS 2000, 1889-1891.

Klein, G., and Sanders, J., 1964. Comparison of sediments from Bay of Fundy and Dutch Wadden Sea tidal flats. Journal of Sedimentary Research 34.

Klemas, V., 2011. Beach profiling and LIDAR bathymetry: an overview with case studies. Journal of Coastal Research 27, 1019-1028.

Lee, C., Yoo, H., Park, K., 1992. Distribution and properties of intertidal surface sediments of Kyeonggi Bay, west coast of Korea. Journal of the Oceanological Society of Korea 27, 277-289.

Lee, H., Chu, Y., Park, Y., 1999. Sedimentary processes of fine-grained material and the effect of seawall construction in the Daeho macrotidal flat–nearshore area, northern west coast of Korea. Marine Geology 157, 171-184.

Lee, H., Chun, S., Chang, J., Han, S., 1994. Landward migration of isolated shelly sand ridge (chenier) on the macrotidal flat of Gomso Bay, west coast of Korea: controls of storms and typhoon. Journal of Sedimentary Research 64.

Lee, H., Ahn, K., Kim, D., 2010. DEM generation of tidal flat by the area based matching method using digital aerial stereo images. Journal of the Korean Association of Geographic Information Studies 13, 42-52.

Lee, H., Han, D., Ahn, K., 2011. Change estimation of tidal flat elevation of Suncheon Bay using aerial images. Journal of Korean Society of Envirionmental Technology 12, 223-229.

Lee, Y., Ryu, J., Choi, J., Soh, J., Eom, J., Won, J., 2011. A Study of decadal sedimentation trend changes by waterline comparisons within the Ganghwa tidal flats initiated by human activities. Journal of Coastal Research 27, 857-869.

Liu, Y., Li, M., Cheng, L., Li, F., Chen, K., 2012. Topographic mapping of offshore sandbank tidal flats using the waterline detection method: A case study on the Dongsha Sandbank of Jiangsu Radial Tidal Sand Ridges, China. Marine Geodesy 35, 362-378.

Mason, D., Davenport, I., Robinson, G., Flather, R., McCartney, B., 1995. Construction of an inter-tidal digital elevation model by the 'Water-Line'Method. Geophysical Research Letters 22, 3187-3190.

Mason, D., Gurney, C., Kennett, M., 2000. Beach topography mapping - a comparsion of techniques. Journal of Coastal Conservation 6, 113-124.

Mason, D., Hill, D., Davenport, I., Flather, R., Robinson, G., 1997. Improving inter-tidal digital elevation models constructed by the waterline technique. European Space Agency-Publications-Esa SP 414, 1079-1082.

Milliman, J., Shen, H., Yang, Z., Mead, R., 1985. Transport and deposition of river sediment in the Changjiang estuary and adjacent continental shelf. Continental Shelf Research 4, 37-45.

Niedermeier, A., Hoja, D., Lehner, S., 2005. Topography and morphodynamics in the German Bight using SAR and optical remote sensing data. Ocean Dynamics 55, 100-109.

Phinn, S., Menges, C., Hill, G., Stanford, M., 2000. Optimizing remotely sensed solutions for monitoring, modeling, and managing coastal environments. Remote Sensing of Environment 73, 117– 132.

Postma, H., 1961. Transport and accumulation of suspended matter in the Dutch Wadden Sea. Netherlands Journal of Sea Research 1, 148-190.

Rogers, A., and Ingalls, R., 1969. Venus: Mapping the surface reflectivity by radar interferometry, Science 65, 797-799.

Ryu, J., Kim, C., Lee, Y., Won, J., Chun, S., Lee, S., 2008. Detecting the intertidal morphologic change using satellite data. Estuarine, Coastal and Shelf Science 78, 623-632.

Ryu, J., Won, J., Min, K., 2002. Waterline extraction from Landsat TM data in a tidal flat: a case study in Gomso Bay, Korea. Remote Sensing of Environment 83, 442-456.

Ryu, S., You, H., Lee, J., 1999. Seasonal variation of surface sediments and accumulation rate on the intertidal flats in Hampyong Bay, southwestern coast of Korea. The Sea 4, 127-135.

Ryu, S., Yu, H., 1997. Distribution pattern and characteristics of the surface sediments in Hampyong Bay, the southwestern coast of Korea. Journal of the Korean earth science society 18, 367-367.

Ryu, S., 2003. Seasonal variation of sedimentary processes in a semi-enclosed bay: Hampyong bay, Korea. Estuarine, Coastal and Shelf Science 56, 481-492.

Sallenger, A., Krabill, W., Swift, R., Brock, J., List, J., Hansen, M., Holman,

R., Manizade, S., Sontag, J., Meredith, A., 2003. Evaluation of airborne topographic lidar for quantifying beach changes. Journal of Coastal Research 19, 125-133.
Schwabisch, M., Lehner, S., Winkel, N., 1997. Coastline extraction using ERS SAR Interferometry. Proceedings Third ERS Symposium, Florence, Italy.
Sibson, R., 1981. A brief description of natural neighbour interpolation. Interpreting multivariate data 21, 21-36.
Stockdonf, H., Sallenger J., List, J., Holman, R., 2002. Estimation of shoreline position and change using airborne topographic lidar data. Journal of Coastal Research, 502-513.
Van Stokkom, H., Stokman, G., Hovenier, J., 1993. Quantitative use of passive optical remote sensing over coastal and inland water bodies. International Journal of Remote Sensing 14, 541-563.
Van Straaten, L., Kuenen, P., 1957. Accumulation of Fine Grained Sediments in the Dutch Waddensea.
Wang, Y., Zhang, R., Gao, S., 1999. Velocity variations in salt marsh creeks, Jiangsu, China. Journal of coastal research, 471-477.
Waska, H., Kim, G., 2010. Differences in microphytobenthos and macrofaunal abundances associated with groundwater discharge in the intertidal zone. Marine Ecology Progress Series 407, 159-172.
Wegműller, U., Werner, C., Strozzi, T., Wiesmann, C., 2005. ERS-ASAR integration in the interferometric point target analysis, Proceedings of FRINGE 2005 Workshop, Frascati, Italy.
Werner, M., 2000. Shuttle Radar Topography Mission (SRTM) - Mission Overview, EUSAR 2000, 209-212.
Werner, M., Klein, K., Haeusler, M., 2000. Performance of the Shuttle Radar Topography Mission, X-Band Radar System. Proceedings of IGARSS 2000, 2590-2592.
Welch, R., Remillard, M., Alberts, J., 1992. Integration of GPS, remote sensing, and GIS techniques for coastal resource management. Photogrammetric Engineering and Remote Sensing 58, 1571-1578.
Wells, J., Adams, C., Park, Y., Frankenberg, E., 1990. Morphology sedimentology and tidal channel processes on a high-tide-range mudflat, west coast of South Korea. Marine Geology 95, 111-130.
Wells, J., and Coleman, J., 1981. Physical processes and fine-grained sediment dynamics, coast of Surinam, South America. Journal of Sedimentary Research 51.
Wimmer, C., Siegmund, R., Schwabisch, M., Moreira, J., 2000. Generation of high precision DEMs of the Wadden Sea with airborne interferometric SAR. Geoscience and Remote Sensing, IEEE Transactions on 38, 2234-2245.

Yang, B., and Chun, S., 2001. A seasonal model of surface sedimentation on the Baeksu open-coast intertidal flat, southwestern coast of Korea. Geosciences Journal 5, 251-262.

Yoo, H., Bae, I., Ryu, J., Ahn, Y., 2005. A study of the sedimentrary environments in the Korean tidal flat using Landsat TM/ETM+, Kompsat EOC, and IKONOS. Proceddings of IGARSS 2005, 3.

Zebker, H.,Werner, C., Rogen, P., Hensley, S., 1994. Accuracy of topographic maps derived from ERS-1 interferometric radar. IEEE Transactions on Geoscience and Remote Sensing 32, 823-836.

Zhao, B., Guo, H., Yan, Y., Wang, Q., Li, B., 2008. A simple waterline approach for tidelands using multi-temporal satellite images: a case study in the Yangtze Delta. Estuarine, Coastal and Shelf Science 77, 134-142.

국문요약

조간대는 평균간조선과 평균만조선 사이에 위치하는 완경사의 대지로서 지형학적, 지질학적 및 생물·생태학적 측면에서 중요한 작용을 한다. 최근 대규모 간척사업, 해수면 상승 등 여러 가지 요인에 의해 해안환경이 급속도로 변화되고 있다. 이러한 변화를 효과적으로 탐지하고 모니터링하는 수단으로 원격탐사자료를 기반으로 waterline 기법이 널리 이용되고 있다. 또한, waterline 기법은 과거 조간대의 지형정보(DEM)을 생성할 수 있는 효과적인 방법이라고 할 수 있다. 본 연구에서는 원격탐사 자료를 활용하여 한국 서해안의 곰소만과 함평만 조간대에 대한 지형변화를 관측하고자 한다.

우선, 본 연구에서는 2003년과 2004년 여름철(6월~8월)과 겨울철(12월~2월)에 촬영한 18장의 Landsat 7 위성영상을 이용하여 해안선을 추출하였고, waterline 기법을 적용하여 여름철과 겨울철에 해당되는 DEM을 각각 생성하였다. 생성된 여름철과 겨울철의 DEM을 이용하여 계절변화에 의한 해안지형 변화를 정량적으로 산출하였다. 그 결과, 곰소만에서는 여름철 퇴적(summer deposition)이 우세하였고 약 12.8cm의 지형변화가 발생하였다. 반면, 함평만에서는 여름철 침식(summer erosion)이 우세하는 것으로 나타냈고 약 −5.0 cm의 지형변화가 발생하였다. 곰소만과 함평만은 같은 종류의 반폐쇄적인(semi−closed tidal

flats) 조간대임에도 불구하고 퇴적과 침식의 양상은 서로 반대의 경향을 보여준다. 그 원인은 곰소만과 함평만의 다른 퇴적상과 만의 형태에 의해 서로 다른 지형변화가 나타나는 것으로 보여진다.

다음, waterline 기법을 적용하여 1980년대부터 2010년대까지 곰소만과 함평만 조간대에 대한 장기간의 지형변화에 대한 분석도 진행되었다. 현재까지 수행된 대부분의 연구들은 시·공간적인 변화에 초점에 맞추어져 있어서 계절변화에 의한 지형변화는 고려되고 있지 않았다. 따라서, 본 연구에서는 계절적인 변화에 의한 조간대의 지형변화까지 고려함으로써, 곰소만과 함평만 지역에 대한 30년간의 정확한 지형변화를 도출하였다. 그 결과, 곰소만에서는 계절에 관계없이 퇴적이 우세하였고, 겨울철과 여름철에 각각 12.4cm 와 31.9cm의 퇴적이 발생하였다. 함평만의 경우, 전체적으로 침식이 우세하였고, 겨울철에는 약 29.6cm의 침식이 발생하였고 여름철에는 41.2cm의 침식이 발생하였다.

추가적으로 곰소만과 함평만에 대해 1980년대부터 10년을 주기로 2010년대까지 82장의 Landsat 위성영상을 사용하여, 시계열적인 지형변화를 관찰하였다. 그 결과, 곰소만과 함평만에서는 모두 여름철보다 겨울철에 퇴적이 우세하는 계절적인 특징이 뚜렷하게 나타났다. 또한, 규칙적인 패턴으로 퇴적 또는 침식을 나타내던 곰소만과 함평만 조간대의 지형변화는 2000년대를 기준으로 비정상적인 패턴을 나타냈다. 그 원인은,

1990년대 중반부터 축조되기 시작한 대규모 간척지-새만금 간척지의 축조에 의한 주변 해역(연구대상지 포함)의 해류와 파향이 변화되어 나타나는 현상으로 보여진다.

마지막으로, 본 연구에서는 SAR 간섭기법을 이용한 조간대의 지형변화 탐지가능성을 파악하였다. 사용된 자료로는 TanDEM-X와 SRTM mission 자료를 이용하였다. SAR 간섭기법으로 생성된 DEM과 waterline기법에 의해 구축된 DEM의 시간적인 불일치성의 한계에 의해 양적으로 직접적인 비교는 할 수 없었으나 퇴적과 침식의 경향성은 비교할 수 있었다. 그 결과, 퇴적과 침식에 대한 경향성은 일치한 것으로 나타났으며 SAR 간섭기법을 활용한 조간대 지형변화 탐지가능성을 충분히 확인할 수 있었다. 향후, 보다 많은 bi-static SAR 자료들이 확보된다면 시계열적인 지형변화 분석도 가능할 것으로 보여진다.

주요어 : waterline 기법, 조간대, 계절적인 변화, 지형변화, 원격탐사.

학 번 : 2011-31269